












A single MYB transcription factor with multiple functions during flower development

Mathilde Chopy¹ , Marta Binaghi¹ , Gina Cannarozzi¹ , Rayko Halitschke² , Benoît Boachon³ , Roel Heutink⁴ , Dikki Pedenla Bomzan³ , Lea Jäggi¹ , Geert van Geest⁵ , Julian C. Verdonk⁴  and Cris Kuhlemeier¹ 

¹Institute of Plant Sciences, University of Bern, Altenbergrain 21, 3013, Bern, Switzerland; ²Department of Mass Spectrometry and Metabolomics, Max-Planck-Institute for Chemical Ecology, Hans-Knöll-Str. 8, 07745, Jena, Germany; ³CNRS, LBVpam UMR 5079, Université Jean Monnet Saint-Etienne, F-42023, Saint-Etienne, France; ⁴Horticulture and Product Physiology, Plant Science Group, Wageningen University and Research, 6708, Wageningen, the Netherlands; ⁵Interfaculty Bioinformatics Unit, University of Bern, Baltzerstrasse 6, 3012, Bern, Switzerland

Summary

Author for correspondence:
Cris Kuhlemeier
Email: cris.kuhlemeier@ips.unibe.ch

Received: 14 February 2023
Accepted: 22 May 2023

New Phytologist (2023)
doi: 10.1111/nph.19096

Key words: flower development, flower maturation, *Petunia*, R2R3-MYB transcription factors, senescence, starch metabolism, terpenoids/isoprenoids/carotenoids, volatile compounds.

- Members of the R2R3-MYB transcription factor subgroup 19 (SG19) have been extensively studied in multiple plant species using different silenced or mutated lines. Some studies have proposed a function in flower opening, others in floral organ development/maturation, or specialized metabolism production. While SG19 members are clearly key players during flower development and maturation, the resulting picture is complex, confusing our understanding in how SG19 genes function.
- To clarify the function of the SG19 transcription factors, we used a single system, *Petunia axillaris*, and targeted its two SG19 members (*EOB1* and *EOB2*) by CRISPR-Cas9.
- Although *EOB1* and *EOB2* are highly similar, they display radically different mutant phenotypes. *EOB1* has a specific role in scent emission while *EOB2* has pleiotropic functions during flower development. The *eob2* knockout mutants reveal that *EOB2* is a repressor of flower bud senescence by inhibiting ethylene production. Moreover, partial loss-of-function mutants (transcriptional activation domain missing) show that *EOB2* is also involved in both petal and pistil maturation through regulation of primary and secondary metabolism.
- Here, we provide new insights into the genetic regulation of flower maturation and senescence. It also emphasizes the function of *EOB2* in the adaptation of plants to specific guilds of pollinators.

Introduction

Flower development can be divided into floral organ identity establishment, growth, maturation, and senescence. Organ identity is established by the combinatorial action of the ABC class genes (Coen & Meyerowitz, 1991), and how it varies between species has been studied in detail (Soltis *et al.*, 2007). Once established, the organs grow out and differentiate to carry out their specific functions in pollinator attraction and reward. After pollination, petals and stamens senesce and seeds are produced within the ovary. Members of subgroup 19 (SG19) of the R2R3-MYB transcription factor family are key players in the later stages of floral organ development and maturation. A number of studies, mainly in Solanaceae and Arabidopsis, have documented their functions in flower opening (Colquhoun *et al.*, 2011; Liu & Thornburg, 2012; Reeves *et al.*, 2012; Niwa *et al.*, 2018; Schubert *et al.*, 2019), senescence (Colquhoun *et al.*, 2011), nectary development (Liu *et al.*, 2009; Liu & Thornburg, 2012; Schmitt *et al.*, 2018), stamen development (Mandaokar *et al.*, 2006;

Cheng *et al.*, 2009; Song *et al.*, 2011; Reeves *et al.*, 2012; Qi *et al.*, 2015; Huang *et al.*, 2017, 2020; Battat *et al.*, 2019), ovule fertility (Schubert *et al.*, 2019), pistil length (Reeves *et al.*, 2012; Schubert *et al.*, 2019; Yarahmadov *et al.*, 2020), as well as production of secondary metabolites such as scent compounds (Spitzer-Rimon *et al.*, 2010, 2012; Van Moerkercke *et al.*, 2012; Medina-Puche *et al.*, 2015; Ke *et al.*, 2021), flavonols or terpenes (Battat *et al.*, 2019; Shan *et al.*, 2020; Yang *et al.*, 2020; C. Zhang *et al.*, 2021; X. Zhang *et al.*, 2021) (Fig. 1a). These later stages have been studied in a variety of species, often with a variety of molecular tools. Consequently, it is often not clear whether contrasting mutant phenotypes are species-specific, or are due to the methods used, to the focus of the study on a particular organ, or to the multifunctionality of the SG19 MYB factors. For example, RNAi lines targeting tobacco *MYB305* led to nectary maturation defects in one study (Liu *et al.*, 2009; Liu & Thornburg, 2012), and to flower opening defects in another study (Colquhoun *et al.*, 2011). Different phenotypes were also observed in *Petunia hybrida*, where targeting *EOB2* by VIGS exclusively affected

scent production (Spitzer-Rimon *et al.*, 2010) whereas RNAi caused flower opening defects (Colquhoun *et al.*, 2011).

The R2R3-MYB SG19 transcription factors are characterized by two main functional domains: an R2R3-MYB domain (RMD^{SG19}) located at the N-terminus and a transcriptional activation domain (TAD) located at the C-terminus (Liu *et al.*, 2009; Schubert *et al.*, 2019; Z. Wu *et al.*, 2021) (Fig. 1b). The RMD^{SG19} and the TAD molecular functions have been individually characterized using different experimental and computational techniques. In summary, the RMD^{SG19} has at least three roles: (1) interact with different proteins (bHLHs, JAZs, DELLAs, ...) (Song *et al.*, 2011; Qi *et al.*, 2015; Huang *et al.*, 2017, 2020; Liu *et al.*, 2017; Schubert *et al.*, 2019; Yang *et al.*, 2020; Ke *et al.*, 2021; X. Zhang *et al.*, 2021); (2) bind DNA through the recognition of particular *cis*-element targets ([G/A]TT[A/T]GG[T/C]) (Weirauch *et al.*, 2014; Medina-Puche *et al.*, 2015); and (3) reach the nucleus through the nuclear localization signal (NLS) (Liu *et al.*, 2009). On the contrary, the TAD recruits the transcriptional machinery and through synergic action, the TAD and RMD, regulate the expression of a wide range of targets (Sablowski *et al.*, 1994; Moyano *et al.*, 1996; Liu *et al.*, 2009; Spitzer-Rimon *et al.*, 2010; Moerkercke *et al.*, 2011; Liu & Thornburg, 2012; Medina-Puche *et al.*, 2015; Battat *et al.*, 2019; Kurilla *et al.*, 2019; Yang *et al.*, 2020; Bian *et al.*, 2021; Ke *et al.*, 2021; C. Zhang *et al.*, 2021; X. Zhang *et al.*, 2021; Z. Wu *et al.*, 2021; Wang *et al.*, 2022) (Supporting Information Tables S1, S2). R2R3-MYB SG19 protein sequences have the typical features of transcriptional activators. No characteristic repression motifs (EAR or TLLRF) (Ma & Constabel, 2019) were found and all the targets identified in the literature (except one) were directly activated by R2R3-MYB SG19 members (Table S2). According to these results, SG19 members associate with a plethora of interacting proteins and promoters providing the potential to regulate many different processes of flower development.

The complex and conflicting data on the function of SG19s during flower development necessitate an in-depth structural and functional characterization of its members. To do so, we used a single system, *P. axillaris*, where two members of the SG19 clade have been identified: EMISSION OF BENZENOIDS I and II (EOB1 and EOB2). Those two genes have a flower-specific expression pattern. We generated mutations in *EOB1* and *EOB2*

using CRISPR-Cas9, and analyzed their different functions. Domain-mutants also reveal the specific contributions of the two domains, RMD^{SG19} and TAD, in EOB2 functions. These discoveries made it clear that EOB2 is a complex multifunctional protein during floral organ development. Our study contributes to explain the complexity of the R2R3-MYB SG19-associated functions observed within and between species and in a broader perspective to study flower maturation.

Materials and Methods

Plant material and growth conditions

Petunia axillaris (Lam.) *ssp. axillaris* P (referred to as *P. ax* P or WT) originates from the University of Bern Botanical Garden (Hoballah *et al.*, 2005). Plants were grown in a growth chamber under a light : dark regime of 15 h : 9 h at 22°C : 17°C, in commercial soil (70% Klasman substrate, 15% Seramis clay granules, 15% quartz sand), and fertilized once a week with a nitrogen–phosphorous–potassium and iron fertilizer.

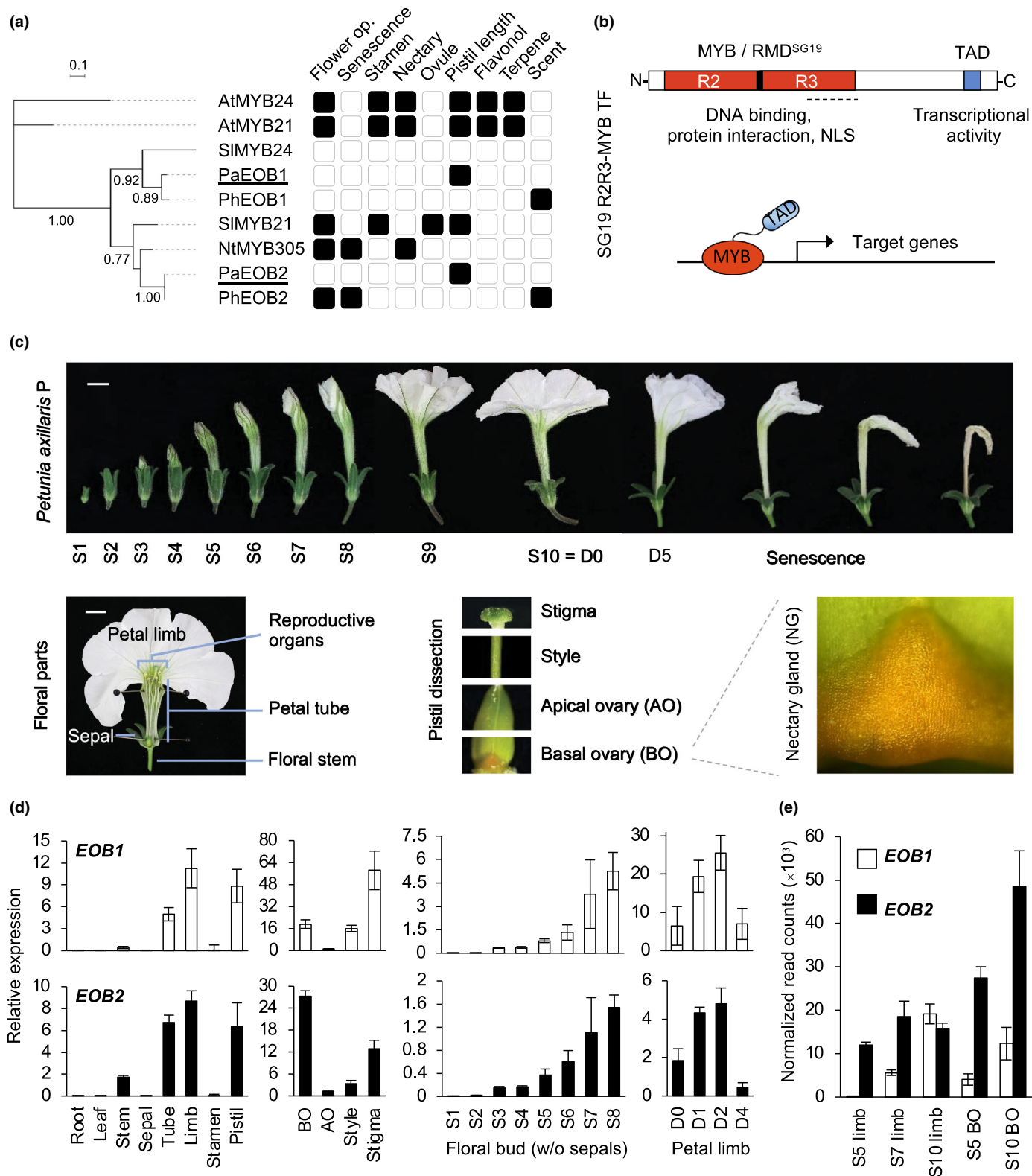
Generation of phylogenetic tree

Phylogenetic reconstruction focused on R2R3-MYB subgroup 19 from *Arabidopsis thaliana* (At), *Solanum lycopersicum* (Sl), *Nicotiana tabacum* (Nt), *Petunia hybrida* (Ph), and *Petunia axillaris* (Pax). Protein sequences alignment was performed with the plug-in version of MUSCLE for UGENE, v.40.1, default parameters (Edgar, 2004; Okonechnikov *et al.*, 2012). Tree was built with PHYML v.20 120 412 in UGENE, with LG substitution matrix, branch support calculated with SH-like method (Guindon *et al.*, 2010).

Vectors construction

The CRISPR-Cas9 Vectors (pHSE401, dual gRNA), called VB191229-3063hgg and VB190510-1037erq targeting *EOB1* or *EOB2*, respectively, were commercially synthesized by Vector-Builder (<https://en.vectorbuilder.com/design/retrieve.html>). For each vector, two unique gRNAs were selected (gRNA sequences are listed in Table S3).

Fig. 1 Analysis of the R2R3-MYB Subgroup 19 (SG19) family complexity and focus on *Petunia axillaris* EOB1 and EOB2 members. (a) Phylogenetic analysis of members of the SG19 R2R3-MYB in *Arabidopsis thaliana* (At), *Solanum lycopersicum* (Sl), *Nicotiana tabacum* (Nt), *Petunia hybrida* (Ph) and *Petunia axillaris* (Pax). Numbers at nodes represent bootstrap values and scale bar indicates the number of amino acid substitutions per site. Gene functions reported in the literature are indicated by black squares in the associated table (flower opening, flower senescence, stamen development, nectary development, ovule development, pistil length, flavonol, terpene, and scent production). (b) Diagram describing the SG19 R2R3-MYB protein structure with domain organization. The R2R3-MYB domain (RMD^{SG19}) is represented in red and the C-terminal motif NyWS^V/_M^E/_D^D/_LW^P/_S which is a transcriptional activation domain (TAD) in blue. The RMD^{SG19} is involved in DNA binding of specific target genes, protein–protein interactions (with repressor proteins such as DELLAs, JAZs, or bHLHs) and contains a nuclear localization signal (NLS) (see Supporting Information Tables S1, S2 for more details). The dashed line below the RMD^{SG19} represents the position of the putative bipartite NLS. The R2R3-MYB domain binds DNA and the TAD activates the target genes. (c) Floral developmental stages, floral parts and pistil parts of *P. axillaris* used in this study. Bars, 1 cm. S1 to S10 = Stage 1 to Stage 10, more details about stages are available on Fig. S3. (d) RT-qPCR analysis of *EOB1* and *EOB2* expression in *P. axillaris* P. The different floral tissues have been dissected from open flower (S10). AO, Apical ovary; BO, Basal ovary; D0–D4, number of days post anthesis; Stem, floral stem. Relative expression values are means of three biological replicates with SD, normalized against *ACT11* and *RAN1*. (e) RNA sequencing analysis of *EOB1* and *EOB2* expression in petal limb and basal ovaries (BO) at different stages (details are available in Table S5).



Petunia axillaris P stable transformation with *Agrobacterium*

Stable transformation procedure is based on a classical transformation protocol (Chopy *et al.*, 2020) with some modifications.

Briefly, leaves from 4–6-wk-old plants of *P. axillaris* P were surface sterilized and cut with a scalpel blade into one cm² small pieces. Sterilized leaf disks were put in a liquid *A. tumefaciens* (strain LBA4404) suspension for 30 min, dried between two layers of sterile filter papers and transferred to a coculture plate

medium for 5 d at 24°C (in the dark with a progressive increase of light). Then, once a week, leaf fragments were transferred to a fresh selective medium containing the appropriate selection agent and were kept at 24°C with moderate light, under long day conditions until the apparition of shoots. Each individual shoot was excised from the calli and transferred to a rooting medium. After rooting, plants were transplanted to soil and grown in a growth chamber. The screening was then performed on these plants after one week to allow them to acclimatize to the soil conditions.

Overexpression constructs and transient expression

The full-length cDNAs of *EOB1*, *EOB2*, *eob2-2*, and *eob2-3* from *P. axillaris* wild-type, *eob2-2* or *eob2-3* were cloned (Table S4) in the pDONR221 vector (Invitrogen) and transferred to the pGWB402 vector (Nakagawa *et al.*, 2007). Transient transformation of *Petunia axillaris* P leaves using *A. tumefaciens* (strain GV3101) was performed as described previously (Moerkercke *et al.*, 2011) with some modifications. *Petunia* leaves from 4–6-wk-old plants were syringe-infiltrated. Three days later, four replicates per construct were harvested (one replicate consists of three leaf disks of 8 mm of diameter near to the agroinfiltrated position) and RT-qPCR were performed using *RAN1* as reference gene.

DNA extraction and genotyping

Genomic DNA was extracted from fresh leaf samples using a modified SDS extraction protocol (Edwards *et al.*, 1991). Primer pairs used for the genotyping are listed in Table S4.

Color images

Flower and branch images were recorded with a Canon EOS 60D camera and Canon 35 mm lens. Floral organ pictures were photographed under a stereoscopic microscope (SMZ1500; Nikon, Tokyo, Japan) equipped with a camera (DMC6200; Leica, Wetzlar, Germany).

Phenotypic measurements

Before phenotyping, the *eob1* or *eob2* single homozygous mutants or heterozygous lines, cas9-negative lines were selected and we confirmed by sequencing that our gRNAs specifically targeted either *EOB1* or *EOB2*. Phenotypic measurements included tube length, opening angle, limb area, nectar volume, and scent emission. All the flowers used for phenotyping were harvested 1 d postanthesis right before the onset of dark in the growth chamber.

Petal morphological traits (tube length, opening angle, and limb area) were measured by photographing front and side view of 12 flowers per genotype. Images were analyzed using the IMAGEJ software. Nectar volumes were quantified according to the protocol described previously (Brandenburg *et al.*, 2012). Methylbenzoate and benzaldehyde compounds were analyzed as described previously by proton transfer reaction mass spectrometry (PTR-MS; Ionicon®, Innsbruck, Austria) (Amrad *et al.*, 2016). Five flowers per plant were analyzed as biological replicates.

RNA extractions, cDNA preparation, and quantitative RT-PCR

The different tissue samples used in this study were collected in three biological replicates and stored at –80°C until further processing. RNA extractions were performed using an innuPREP DNA/RNA Mini Kit (Analytik Jena, Jena, Germany; code 845-KS-20800250). cDNA was synthesized using the qScriber cDNA synthesis kit (HighQu, Kraichtal, Germany; code RTK0104) and for RT-qPCR the ORA SEE qPCR Green ROX L mix (HighQu; code QPD0505) was used according to the manufacturer's recommendations. The amplification was performed using a QUANTSTUDIO 5 Real-Time PCR Instrument 346 (Applied Biosystems, Norwalk, CT, USA). The reference genes used to analyze the data were *RAN1* and *ACTIN11* (Mallona *et al.*, 2010). Primer pairs are listed in Table S4.

RNA sequencing

Total RNA was isolated from tissues listed in Table S5 using an innuPREP DNA/RNA Mini Kit (Analytik Jena; code: 845-KS-20800250). The quantity and quality of the purified total RNA was assessed using a Thermo Fisher Scientific Qubit 4.0 fluorometer with the Qubit RNA BR Assay Kit (Q10211; Thermo Fisher Scientific, Chino, CA, USA) and an Advanced Analytical Fragment Analyzer System using a Fragment Analyzer RNA Kit (DNF-471; Agilent, Santa Clara, CA, USA), respectively. Sequencing libraries were made using an Illumina TruSeq Stranded mRNA Library Prep kit (20020595; Illumina, San Diego, CA, USA) in combination with TruSeq RNA UD Indexes (20022371; Illumina) according to Illumina's guidelines. Pooled cDNA libraries were sequenced paired-end using a shared Illumina NovaSeq 6000 S1 Reagent Kit (200 cycles, 20028318; Illumina) on an Illumina NovaSeq 6000 instrument. The run produced a minimum of 36 million reads per sample. The quality of the sequencing run was assessed using Illumina Sequencing Analysis Viewer (Illumina v.2.4.7) and all base call files were demultiplexed and converted into FASTQ files using Illumina BCL2FASTQ conversion software v.2.20. The quality control assessments, generation of libraries, and sequencing were conducted by the Next Generation Sequencing Platform, University of Bern.

Reads processing, differential expression analysis, and GO

The quality of the RNA-seq reads was assessed using FASTQC v.0.11.9 (Andrews, 2010). Adapters were trimmed with CUTADAPT v.3.4.1 (Martin, 2011). The reads were aligned to the *Petunia axillaris* N reference genome v.4.03 (Peax403; available on NCBI GenBank under the accession no. GCA_026929995.1) using HISAT2 v.2.2.1 (Kim *et al.*, 2015). FEATURECOUNTS v.2.0.1 (Liao *et al.*, 2014) was used to count the number of reads overlapping with each gene as specified in the genome annotation corresponding with Peax403 (gff file can be downloaded from CoGe with the id 62433). The Bioconductor package DESeq2 v.1.36.0 (Love *et al.*, 2014) was used to test for differential gene expression

between the experimental groups. Gene GO-term mappings were obtained from (Patrick *et al.*, 2021), and GO-term enrichment was performed with CLUSTERPROFILER v4.4.4 (T. Wu *et al.*, 2021).

1-MCP treatment

To inhibit ethylene perception, WT, *eob2-1^{KO}*, *eob2-2^{KO}*, and *eob2-3^{LofTAD}* plants were placed in a growth chamber (Percival, model: E-36L2) and treated with an ethylene receptor antagonist, 1-MCP (1-methylcyclopropene) volatile treatment. To treat the plants, two EthylBloc™ Sachets of 2.5 g (AgroFresh, Philadelphia, PA, USA) were used and replaced once a day during at least 2 wk.

Ethylene measurements

Ethylene measurements were taken using a laser-based photoacoustic ethylene sensor (ETD-300, SensorSense, Nijmegen, the Netherlands). For WT and *eob2-1^{KO}* ethylene measurements, full flower buds, dissected petals, or pistils at Stage 5 were used (three flowers per plant were analyzed as biological replicates, for WT $n = 30$ and for *eob2-1^{KO}* $n = 45$). Mutant samples were collected before the first signs of senescence, when the petal tips were still rigid. Flower buds or dissected organs were enclosed in 4-ml vials and an accumulation time of 5 h was used between harvest time and measurements. Ethylene concentrations were analyzed with a flow rate of 2.51 h^{-1} and quantified by signal integration after curve fitting. Ethylene concentrations were calculated based on measurements of a 500-ppb ethylene gas standard analyzed as a reference sample.

Quantification of sesquiterpene accumulation in *Petunia* pistils and emission from tube

Experiments were essentially performed as previously described (Boachon *et al.*, 2019). For the quantification of sesquiterpenes accumulation in pistils, 10 pistils per plant line were harvested at flower stage S9 and placed in 3 ml hexane. Camphor (3 nM) was added as internal standard (IS). Tissues were crushed in hexane with a potter, vortexed for 20 s, sonicated for 10 min at 40°C , and centrifuged at 2000 g for 5 min. Supernatant was recovered, concentrated under nitrogen flow to $c. 300 \mu\text{l}$, and analyzed by GC–MS (for more details see Methods S1).

For the analysis of sesquiterpene emission from the inner surface of the *Petunia* tube, *Petunia* flowers at stage S9 were detached from their receptacle, their reproductive organs were carefully removed with forceps and flowers were placed in 5% sucrose solution. Emitted sesquiterpenes were collected by Stir Bar Sorptive Extraction (SBSE) by placing a magnetic Twister® (Gerstel, Mülheim, Germany) coated with Polydimethylsiloxane (PDMS) placed inside the upper part of the *Petunia* tube. After 48 h of collection, Twisters were eluted with $200 \mu\text{l}$ of hexane containing 2 nmol of IS, vortexed for 10 s and samples were analyzed by GC–MS (for more details, see Methods S1).

Starch and carotenoid measurements

Tissues collected for the analysis are described in Table S6. The secreted nectar from WT ovaries was removed as much as possible using a tissue. WT and *eob2-3^{LofTAD}* ovaries were cut just above the nectary glands. Limb and basal ovary samples were immediately flash-frozen in liquid nitrogen and stored at -80°C . Frozen samples were lyophilized using a Freeze Dry system (Lyquest, from Swiss Vacuum technologies) for 4 d at -50°C , 10 mbar, in the dark.

Carotenoids were extracted from $c. 10 \text{ mg}$ of freeze-dried nectaries and petals. Quantification of carotenoids was carried out with an HPLC system (UltiMate 3000; Thermo Fisher Scientific) (for more details, see Methods S2). Carbohydrates were extracted and quantified from a $c. 3 \text{ mg}$ freeze-dried, ball-milled, tissues with 1 ml of 80% ethanol for 20 min at 80°C according to Van Geest *et al.* (2016) with modifications (see Methods S3).

Detection of starch by Lugol staining

Ovaries were placed in Lugol's solution (N052; Carl Roth, Karlsruhe, Germany) and a vacuum infiltration of 1 min was applied followed by a 10-min incubation. Samples were briefly rinsed with water before being photographed under a stereoscopic microscope (SMZ1500; Nikon) equipped with a camera (DMC6200; Leica). Flowers (w/o sepals) were cleared in 70% ethanol at 80°C for 15 min, progressively rehydrated, stained with Lugol's solution (N052; Carl Roth) for 10 min, and rinsed in water. Pictures were taken before and after staining using a Canon EOS 60D camera and Canon 35 mm lens. For cellular resolution, images of the epidermal peel of petal limbs were captured with an optical microscope (DM2000 LED; Leica).

Confocal microscopy, imaging of epidermal cells, and cell size measurements

Epidermal peels were taken from the outer rim area of the petal limb and placed on microscopy slides for confocal microscopy imaging. Epidermal peels of three flowers per line were taken for comparison. Images were taken with a laser scanning microscope 55 (SP5; Leica) using the differential interference contrast (DIC).

Protein structure prediction

The protein structures of EOB2 and *eob2-2^{KO}* were predicted by AlphaFold (Jumper *et al.*, 2021). The structures were visualized and aligned by PyMOL (v.2.5.3, Schrödinger LLC).

Microsynteny analysis

The microsynteny analysis was performed using GEVO tool from CoGe (Lyons *et al.*, 2008), with PEAX4.03 genome for *P. axillaris* and ITAG release 2.4 genome for *S. lycopersicum*.

Conserved *cis*-elements screening

The promoter sequences of the selected genes were extracted (2 kb upstream of the ATG) and scanned for EOB2 homolog-binding profile matrices (MA1408.1 and MA1037.1 defined in the JASPAR database), using FIMO v.5.1.0 (Grant *et al.*, 2011). Identified motifs ($P < 1e-4$) were counted <http://meme-suite.org/>.

Results

EOB1 and EOB2 are very similar in sequence and expression

To determine the relationships between members of the SG19 R2R3-MYB family, we performed a phylogenetic analysis (Fig. 1a). SG19 members belonging to the Solanaceae were clearly separated from Arabidopsis. Nevertheless, protein alignments showed that the two main functional domains (RMD^{SG19} and TAD) were highly conserved among the different species and among the different gene copies within species (Figs 1b, S1). Furthermore, microsynteny analysis established that *P. axillaris* *EOB1* and *EOB2* are the orthologs of *S. lycopersicum* *MYB24* and *MYB21*, respectively (Fig. S2).

Next, we performed a detailed analysis of the spatial and temporal expression of *P. axillaris* *EOB1* and *EOB2*. Different tissues and developmental stages of *P. axillaris* (Figs 1c, S3 for definition of stages) were used to perform RT-qPCR of *EOB1* and *EOB2* (Fig. 1d). *EOB1* and *EOB2* expression was detected in the petal tube, petal limb, pistil, and a bit in the floral stem, but not in roots or leaves. Within the pistil, *EOB1* and *EOB2* were highly expressed in the basal ovary (BO) and the stigma, suggesting functions in nectary and stigma development (Fig. 1d). RT-qPCR on floral buds (without sepals) from S1 to S8 and on S10 open limbs from anthesis (D0) to 4 d after anthesis (D4) revealed that *EOB1* and *EOB2* started to be expressed from stage S3/S4, their expression increased over flower development and decreased 4 d after anthesis. However, RNA-sequencing data performed on basal ovaries at S5 and S10 and on petal limbs at S5, S7, and S10 (Fig. 1e) showed that *EOB1* expression is overall lower than that of *EOB2*. Moreover, while *EOB1* and *EOB2* are co-expressed in the flower, *EOB2* expression starts slightly before *EOB1*. Unlike previously thought, *EOB1* and *EOB2* functions are most likely

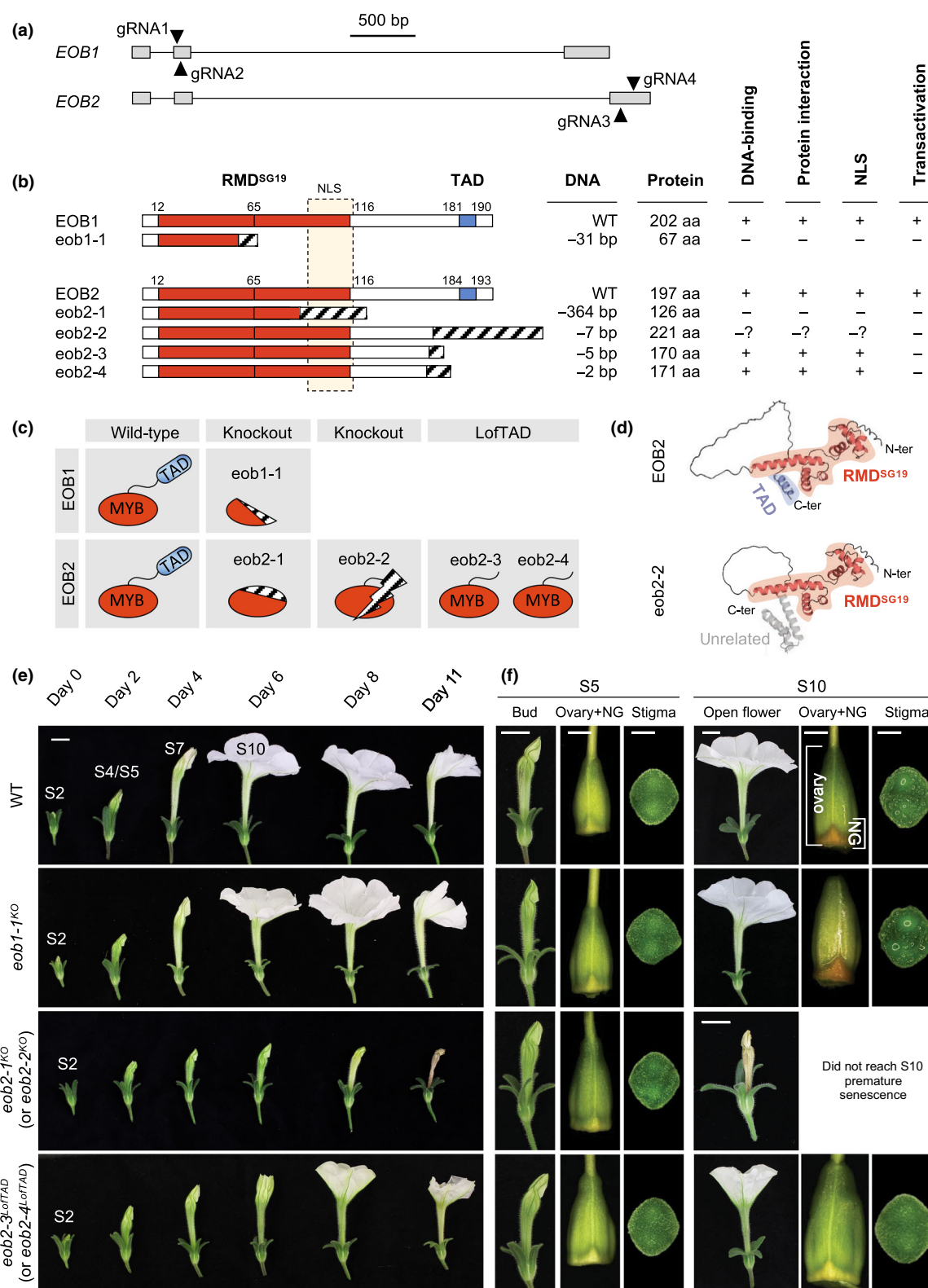
not limited to regulation of the scent pathway and flower opening in *P. axillaris* (Spitzer-Rimon *et al.*, 2010, 2012; Colquhoun *et al.*, 2011).

CRISPR-Cas9 as a tool to decipher R2R3-MYB SG19 complexity

In order to obtain insight into the structure of the proteins, the proteins were characterized based on the literature. *EOB1* and *EOB2* genes encode for transcription factors of 202 and 197 amino acids (aa), respectively, that consist of an RMD^{SG19} at the N-terminal and a TAD at the C-terminal part of the proteins (refer to the Introduction section for more details, Fig. 2b). The RMD^{SG19} was previously shown to contain a nuclear localization signal (NLS). An *in silico* NLS mapper predictor (https://nls-mapper.iab.keio.ac.jp/cgi-bin/NLS_Mapper_form.cgi) (Kosugi *et al.*, 2009) identified a putative bipartite NLS at the end of the RMD^{SG19} (⁸⁹RWSKIAKHLPGRTDNEIKNYWRTRIQKHI K¹¹⁸) in both *EOB1* and *EOB2* (Fig. S1).

To elucidate the molecular and biological functions of *EOB1* and *EOB2* during *P. axillaris* flower development, targeted mutagenesis using CRISPR-Cas9 in *P. axillaris* P background was carried out (Fig. 2a). In total, one allele for *EOB1* and four alleles for *EOB2* were isolated by CRISPR-Cas9 (Fig. 2b; Table S7) and classified in different categories depending on their predicted protein conformations and putative molecular functions (Fig. 2c). The *eob1-1* allele showed a deletion of 31 bp and is predicted to lead to nonfunctional product due to the truncated RMD^{SG19} and the absence of both the NLS and the TAD. The *eob2-1* mutant carried a deletion of 364 bp, which is also expected to cause a complete loss-of-function (Figs 2b,c, S4a,b). The *eob2-2* allele presented a deletion of 7 bp, this frameshift mutation resulted in an abnormal protein product. AlphaFold2 was used to predict the 3D structure of *EOB2* and *eob2-2* proteins (Fig. 2d). The RMD^{SG19} domain was intact in *eob2-2*. By contrast, the C-terminal part of *EOB2* was not conserved in *eob2-2*. This unrelated protein sequence may lead to destabilization of the *eob2-2* protein and disrupt RMD^{SG19} DNA/protein binding capabilities. Even though the *eob2-1* and *eob2-2* encode quite different protein sequences, the two mutants displayed the same strong phenotype (see below). Therefore, most likely *eob2-1* and *eob2-2* both represent knockout alleles, referred as *eob2-1^{KO}* and *eob2-*

Fig. 2 Generation of *EOB2* domain-variants allowed to dissect and characterize *EOB2* domain functions during *Petunia axillaris* flower development. (a) DNA sequences of wild-type *EOB1* and *EOB2*. Exons are shown as grey boxes, solid lines represent introns. Position of the double gRNAs used to target *EOB1* (gRNA1 and gRNA2) and *EOB2* (gRNA3 and gRNA4) are indicated. (b) Diagrams of *EOB1* and *EOB2* wild-type (WT) proteins illustrating the R2R3-MYB domain (RMD^{SG19}) and the transcriptional activation domain (TAD) with their respective amino acid regions, aligned with predicted proteins obtained after CRISPR-Cas9 mutagenesis. Boxes with dashed lines represent unrelated amino acid sequences compared to the wild type. Left: allele names. Right: the DNA column describes the deletions obtained in base pairs (bp) and the protein column predicts the associated protein length in amino acids (aa) followed by the predicted protein activities according to the domain composition (*eob1-1*, *eob2-1*, *eob2-3*, and *eob2-4*) or protein conformation (*eob2-2*). +: active, -: inactive, -: predicted inactive. (c) Diagrams of protein conformation and domains composition of *EOB1* and *EOB2* wild-type and mutant alleles sorted by knockout (KO) and loss-of-TAD (LoFTAD) categories. (d) *EOB2* and *eob2-2* protein structures prediction with AlphaFold, figure was drawn with PyMOL. (e) Pictures of WT, *eob1-1^{KO}*, *eob2-1^{KO}* and *eob2-3^{LoFTAD}* flower development over time. S2 flower buds were used at day 0. No visible phenotype between WT and *eob1-1^{KO}*. Premature senescence observed in *eob2-1^{KO}* (same phenotype for *eob2-2^{KO}*) and juvenile flowers in *eob2-3^{LoFTAD}* (as well as *eob2-4^{LoFTAD}*). (f) Pictures of flower, ovary with nectary glands (NG) and stigma surface of WT, *eob1-1^{KO}*, *eob2-1^{KO}* and *eob2-3^{LoFTAD}* at stage 5 (S5) and stage 10 (S10). Before S5, no differences observed between the different genotypes. After reaching S5, *eob2-1^{KO}* and *eob2-2^{KO}* stop growing and rapidly enter senescence. At S10, *eob2-3^{LoFTAD}* petals did not fully open, stigma surface and nectary were dry and immature compared to the WT or *eob1-1*. Bars: (e) 1 cm (flowers); (f) 1 mm (ovaries and stigmas).



2^{KO} . The *eob2-3* and *eob2-4* alleles contained deletions of 5 bp or 2 bp, respectively. These mutations removed the transcriptional activation domain (TAD) but retained an intact RMD^{SG19} (Fig. 2b,c). The *eob2-3* and *eob2-4* truncated proteins retain the

nuclear localization signal, bind DNA, and can interact with protein partners but lack their transactivation activity. Thus, *eob2-3* and *eob2-4* are referred to as loss-of-TAD alleles (*eob2-3*^{LoFTAD} and *eob2-4*^{LoFTAD}).

EOB2 is a regulator of EOB1

The knockout mutants in *EOB1* and *EOB2* caused very different phenotypes. No visible developmental phenotypes were observed in *eob1-1^{KO}* (Figs 2e,f, 3a), but the emission of the major scent compounds was reduced compared with the wild-type (Fig. 3b) as previously observed in *Petunia hybrida* *EOB1-RNAi* lines (Spitzer-Rimon *et al.*, 2012). Moreover, *IGS* expression was induced in *Petunia* leaves after *EOB1* transient expression (Fig. 3e). We conclude that EOB1 is essential for floral volatile benzenoid/phenylpropanoid (FVBP) production, even in the presence of active EOB2.

The flowers of the *eob2* knockout alleles, *eob2-1^{KO}* and *eob2-2^{KO}*, failed to enter anthesis and prematurely senesced as closed buds. Flower initiation was not affected but flower bud growth was delayed after reaching 2 cm (stage S4) and the buds prematurely entered senescence at 3.5 cm (S5) (Figs 2e,f, 3a, S5). After reaching S5, the flower bud stopped growing and gradually senesced: the petal limb tip started to soften, the flower bud turned yellow/brown and the flower bud was completely brown/dead. At 16 week after germination, the difference between mutant plants and wild-type was remarkable: 100% of fully opened flowers in the wild-type against 0% in the mutant lines (Fig. 3a). As the heterozygotes are phenotypically wild-type, we conclude that the *eob2-1^{KO}* and *eob2-2^{KO}* alleles are recessive (Fig. S6). The fact that expression of *EOB2* precedes *EOB1* expression (Fig. 1e) suggests that EOB2 may be an activator of EOB1. Indeed, *EOB2* expression is independent of EOB1 (Fig. 3c,e) while *EOB1* expression is activated by EOB2 (Fig. 3d,e), probably by binding to the defined 'SG19 MYB-binding site' in the *EOB1* promoter (Figs 3f, S7a). Moreover, no additional effects were observed when comparing the *eob2-2^{KO}* single mutant to the *eob1-1^{KO}/eob2-2^{KO}* double mutant flowers (Figs 3a, S9). Therefore, EOB1 is downstream of EOB2.

The loss-of-TAD mutants display floral organ maturation defects

The *eob2* knockout alleles described so far displayed early senescence and did not reach anthesis, which makes it impossible to investigate EOB2 function(s) beyond Stage 5. Based on its expression pattern (Fig. 1d), *EOB2* may also function in later floral developmental stages. The loss-of-TAD (LofTAD) mutants, *eob2-3^{LofTAD}* and *eob2-4^{LofTAD}*, allowed us to study EOB2 function at the later developmental stages.

The *eob2-3^{LofTAD}* and *eob2-4^{LofTAD}* homozygous single mutants caused identical pleiotropic floral phenotypes with floral organ maturation defects and juvenile characteristics at late stages (Fig. 2f). The *eob2-3^{LofTAD}* mutant was used for further analysis. Compared with the wild-type, petal tubes were shorter, petals did not fully open, limbs were smaller, and had greener petal veins (Fig. 4a,f). Both wild-type and LofTAD limbs were UV-absorbing (Fig. S8). Concerning the reproductive organs, no stamen/pollen phenotypes were observed. By contrast, we noticed phenotypes in style, stigma, and nectary. Styles were twisted, which can be interpreted as an indirect phenotype due to the

mechanical constraints applied by the reduced petal growth (Fig. 4b).

While droplets of exudate were present on wild-type stigmas, the mutant had dry stigma surfaces. A key function of the stigma exudate is pollen hydration, a prerequisite for pollen tube elongation and fertilization. Indeed, *eob2-3^{LofTAD}* failed to hydrate pollen, impairing seed set. Seed yield was increased when the dry *eob2-3^{LofTAD}* stigmas were treated with wild-type stigma exudate (Fig. 4c). Ovule number and development were not impacted (Fig. 4d). After pollination and fertilization, the style was detached from the fruit in the wild-type but not in the mutants (Fig. 4c,e). Nectar secretion was disrupted (Fig. 4g) and carotene levels were reduced (Fig. 4h) indicating defective nectary maturation.

Several SG19 members have been shown to play a role in the production of diverse floral volatiles in a range of species (see the Introduction section). In the *eob2-3^{LofTAD}* petal limbs, benzaldehyde and methylbenzoate were absent, in line with a decreased expression of *ODO1* and *EOB1* (Fig. 4i,j). The emission of terpene volatiles from the floral tube was reduced, as well as their accumulation in the stigma (Fig. 4k,l). In *P. hybrida*, *TPS1* was shown to regulate terpene volatile synthesis and emission from the tube (Boachon *et al.*, 2019). In *eob2-3^{LofTAD}* petal tube, *TPS1* expression was also reduced (Fig. 4m).

Next, we analyzed the F1 progenies. The *eob2-3^{LofTAD}/+* and *eob2-4^{LofTAD}/+* heterozygous flowers displayed an intermediate phenotype (intermediate flower angle opening, nectar volume, and methylbenzoate level) indicating that LofTAD alleles are semidominant (Fig. S6). This intermediate phenotype is compatible with a competition between the products of the wild-type and the LofTAD mutants for the same DNA-*cis*-elements.

EOB2 prevents flower senescence during flower development by inhibiting ethylene synthesis

The contrasting phenotypes of *eob2* knockout vs LofTAD might be explained by differences at the transcriptional level. Therefore, a transcriptome analysis of S5 petal limb from WT, *eob2-1^{KO}* and *eob2-3^{LofTAD}* was carried out (Fig. 5a). *EOB2* expression was significantly downregulated in the knockout line while no significant expression differences were observed in the wild-type vs LofTAD comparison (Fig. S4c). This reinforces the notion that *eob2-1^{KO}* is a complete knockout, while *eob2-3^{LofTAD}* retains partial activity. Whereas 23% of the genes were differentially regulated in the knockout (*eob2-1^{KO}*), only 4.5% were differentially expressed in the LofTAD (*eob2-3^{LofTAD}*). Again, this is in line with partial activity of *eob2-3^{LofTAD}*. Most of the 4.5% were regulated in the same direction (either up- or downregulated) in the two genotypes, supporting that both alleles partly act on the same pathways. Interestingly, in both mutant backgrounds, the majority of the DEGs was upregulated. As structural data strongly indicate that EOB2 is a transcriptional activator (see the Introduction section), the observed upregulation must be an indirect effect (indirect targets and/or mediated by interacting factors). Moreover, an *in silico* scanning promoter analysis revealed that the downregulated gene promoters displayed a significant

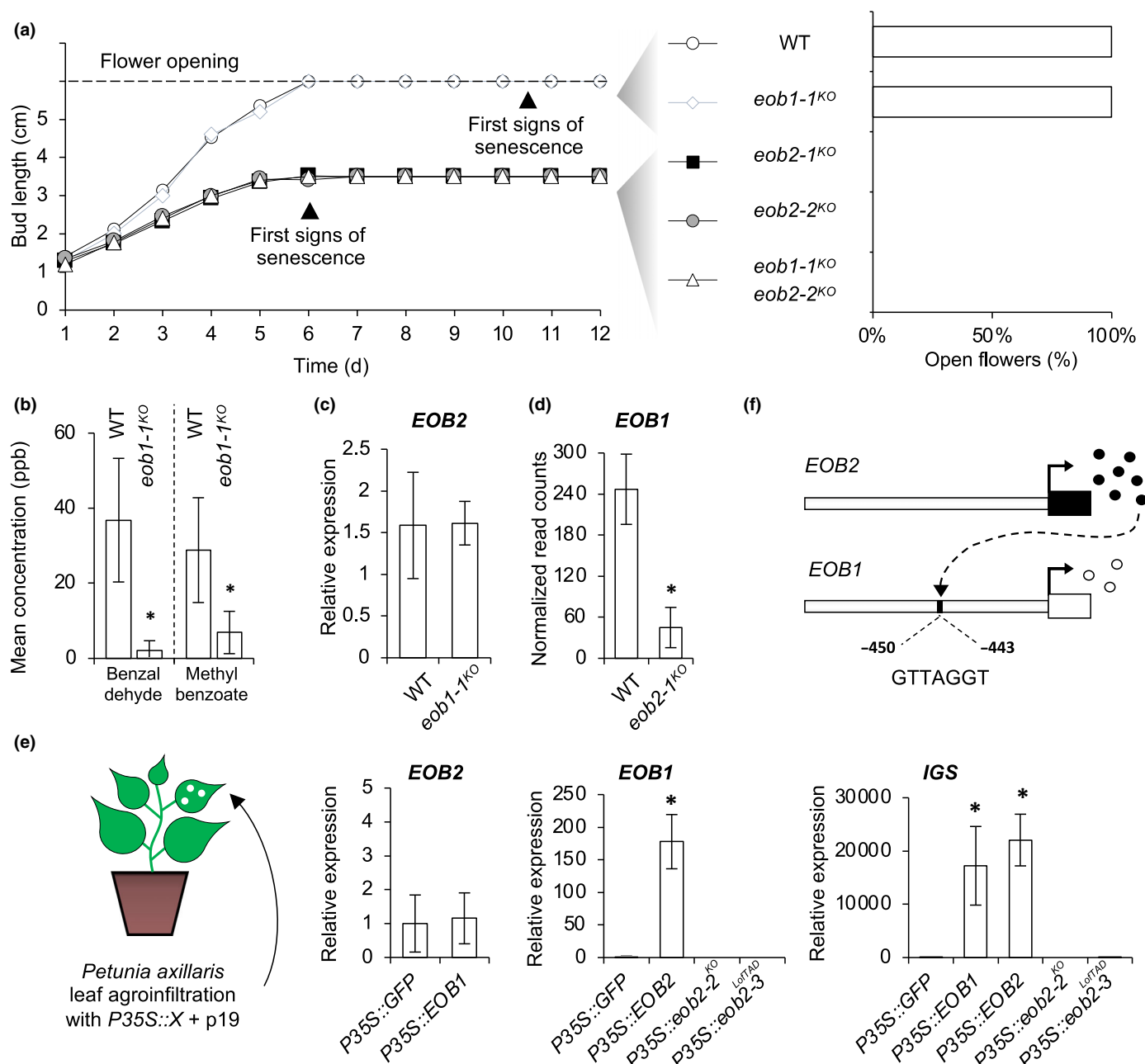


Fig. 3 *EOB2* is a regulator of *EOB1*. (a) Flower growth measurements of WT and crispr mutants from c. 1 cm buds until senescence. Ten flowers per genotype were used for the analysis: WT, *eob1-1^{KO}*, *eob2-1^{KO}*, *eob2-2^{KO}*, and *eob1-1^{KO} eob2-2^{KO}* double mutant. The black arrows indicate the first signs of senescence. The right panel represents the percentage of open flowers 16 wk after germination ($n = 100$). (b) PTR-MS measurements for the major scent compounds, benzaldehyde and methylbenzoate, performed just before dark on 1 d post anthesis (DPA) flowers from WT and *eob1-1^{KO}* plants ($n = 15$; error bars, SD; significant differences Student's t -test: *, $P < 0.05$). (c) RT-qPCR analysis of *EOB2* expression in WT and *eob1-1^{KO}* limb at S10, 1DPA, just before dark ($n = 3$; error bars, SD). (d) RNA sequencing analysis of *EOB1* expression in WT and *eob2-1^{KO}* S5 petal limb ($n = 3$; error bars, SD; significant differences Student's t -test: *, $P < 0.05$). (e) Schematic representation of a *Petunia axillaris* plant showing the extraction of three leaf-disks in the infiltration area. RT-qPCR analysis of *EOB2*, *EOB1* and *IGS* normalized expression in *Petunia axillaris* P leaves, 3 d after agroinfiltration with transient expression constructs ($n = 4$; error bars, SD; significant differences Student's t -test: *, $P < 0.05$). P35S::GFP represents the negative control. (f) Illustration showing a possible interaction between *EOB2* and the promoter of *EOB1*. *EOB1* and *EOB2* promoter sequence analysis (1000 bp before the ATG) revealed the presence of a putative SG19 MYB-binding site 450 bp before the START codon of *EOB1*.

enrichment of the SG19 binding site matrices, while it was not the case for the upregulated gene promoters (Table S8; Fig. S11 see later).

Within the large proportion of *eob2-1^{KO}*-specific DEGs, GO terms associated with senescence were over-represented (Fig. 5b).

Among them, several *ACS* and *ACO* genes encoding enzymes responsible for ethylene synthesis were upregulated (Fig. 5c; Table S9) as well as many ethylene response factors (ERF) and senescence-associated genes (SAG). Genes related to cellular processes maintenance (translation, cellular trafficking, mitotic cell

cycle, etc.) were down-regulated, presumably as a consequence of senescence.

Ethylene is a key hormone promoting flower senescence and blocking ethylene sensitivity partially restored the RNAi-*EOB2*

flower phenotypes in *P. hybrida* and *N. attenuata* (Colquhoun *et al.*, 2011). To obtain direct proof that ethylene production is activated prematurely in *eob2-1^{KO}* and *eob2-2^{KO}* compared to wild-type flowers, we quantified ethylene emission from S5

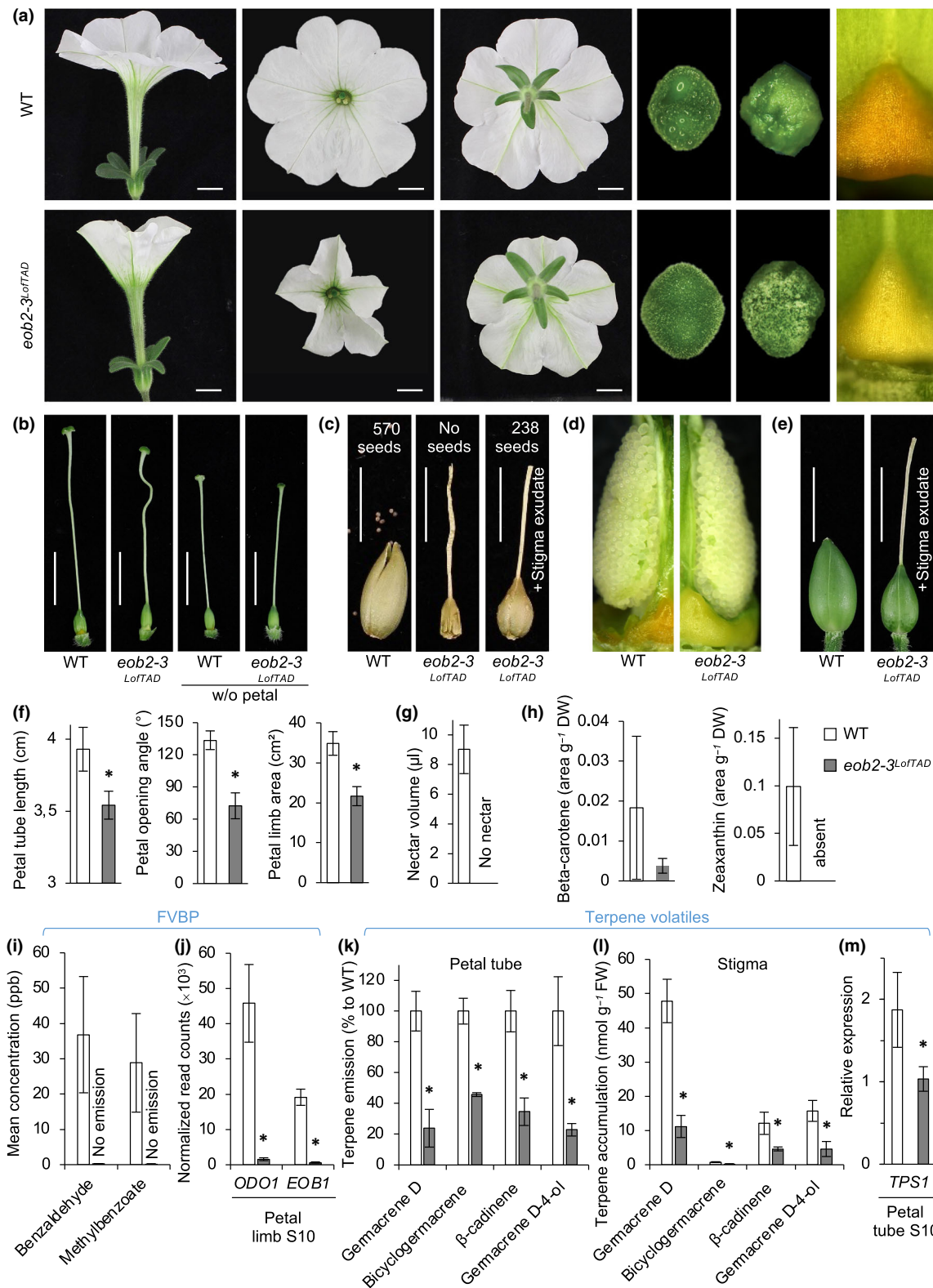


Fig. 4 Different organs impacted in their maturation in *eob2-3^{LofTAD}* mutants. (a) Pictures of WT (top row) and *eob2-3^{LofTAD}* (bottom row) flowers at stage 10 (S10). Side view, top view, bottom view, stigma surface, stigma surface 24 h after pollination of freshly opened flowers and close up of the nectary gland. Bars, 1 cm. (b) Pistil pictures of WT and *eob2-3^{LofTAD}*, 5 d after S3. Left: no petal removal (S10). Right: with petal removal performed at c. S3 (w/o). Twisted styles in *eob2-3^{LofTAD}* are due to petal mechanical constraints. Bars, 1 cm. (c) Capsules one month after pollination. The mean number of seeds per capsule is indicated ($n = 6$). No seeds in the *eob2-3^{LofTAD}* capsule without stigma exudate. Bars, 1 cm. (d) Side view of ovaries with carpel wall removed, comparable number of ovules was observed. (e) Two weeks after pollination the style detached from the fruit/capsule of WT while persisting in *eob2-3^{LofTAD}*. Bars, 1 cm. (f) to (m) WT is represented in white and *eob2-3^{LofTAD}* in dark grey (error bars, SD, except (k) and (l) where error bars, SE; significant differences Student's *t*-test: *, $P < 0.05$). (f) Petal morphological measurements at S10: petal tube length, petal opening angle and petal limb area ($n = 12$). (g) Nectar volume measurements at S10 ($n = 20$). (h) Carotenoid content from nectary at S10. (i) PTR-MS measurements of the two main floral volatiles benzenoid/phenylpropanoid (FVBP) ($n = 15$). (j) RNA-seq of *ODO1* and *EOB1* expression in WT and *eob2-3^{LofTAD}* limb at S10. (k) Terpene volatiles (*TPS1* products) emitted from WT and *eob2-3^{LofTAD}* petal tubes ($n = 5$). (l) Terpene volatiles accumulated on stigmas during anthesis (S9) ($n = 4$). (m) RT-qPCR of *TPS1* from petal tube at S10.

flower buds before the first signs of senescence. Ethylene levels in *eob2-1^{KO}* flower buds at S5 were higher compared to wild-type (Fig. 5d). Since *EOB2* is expressed in both petal and pistil (Fig. 1c), ethylene measurements were performed on dissected petal and pistil from S5 flower buds. We noticed a strong contribution from both floral organs in releasing ethylene. In parallel, a 1-MCP treatment (ethylene action inhibitor) was continuously applied on wild-type, *eob2-1^{KO}* and *eob2-3^{LofTAD}* plants. 1-MCP treatment caused a partial rescue of the *eob2-1^{KO}* flower senescence phenotype but negligible floral developmental effects on wild-type and *eob2-3^{LofTAD}* (Figs 5e, S9, S10). Similar results were obtained with the other allele *eob2-2^{KO}*. Though *eob2-1^{KO}* or *eob2-2^{KO}* flowers reached anthesis after 1-MCP treatment, they did not fully open, were scentless and morphologically similar to *eob2-3^{LofTAD}* or *eob2-4^{LofTAD}* flowers.

EOB2 activates pathways of secondary metabolism

We took advantage of the powerful *eob2-3^{LofTAD}* mutant to (1) identify EOB2 transcriptional targets and (2) unravel to what extent nectary and petal limb maturation are regulated by the same genetic pathway. To do so, we compared the transcriptomes of wild-type and *eob2-3^{LofTAD}* petal limb and nectary, at S5 and S10 (Fig. 6a). The analysis of the differentially expressed genes (DEGs) revealed a higher proportion of upregulated genes in each condition and the number of DEGs was higher at S10 than S5 in both floral organs (Fig. 6a). Since EOB2 is thought to be a transcriptional activator (see the Introduction section), the downregulated genes are potential direct targets. Among the downregulated genes, a significant enrichment of promoters presented SG19 binding sites, which was not the case for the upregulated genes (Figs 6b, S11; Table S8). Sixty genes were commonly downregulated in the four different conditions (Fig. 6c). Among them, we found seven genes encoding enzymes of the shikimate/phenylpropanoid and four carotenoid biosynthetic genes (Fig. 6d). These genes are likely to be direct targets of EOB2 and to support this founding some homologs were also identified as direct targets in other species (Table S2). Indeed, SG19 binding sites were identified at least once in each of the 11 promoters tested, while only five promoters presented the exact motif characteristic for SG19 (Fig. 6d). These data provide evidence that EOB2 is a direct activator candidate of genes involved in shikimate, phenylpropanoid, and carotenoid maturation pathways in both limb and nectary tissues (Fig. S12).

Carbohydrate metabolism is involved in floral organ maturation

Nectary and limb are mostly sink tissues, dependent on the surrounding photosynthetic tissues to provide carbohydrates for their active growth. Starch that is stored at early stages is mobilized later to support respiration, growth, and maturation (Streb & Zeeman, 2012). A GO-term enrichment analysis was performed on the downregulated genes from the four conditions. Only two GO-terms were significantly co-enriched in the four conditions: 'TCA cycle' and 'glycolytic process', meaning that high-energy carbohydrate breakdown was impaired in both *eob2-3^{LofTAD}* nectary and limb (Fig. 7a). We also evaluated whether other components of carbohydrate metabolism were impacted. One gene encoding a beta-amylase (*BAM*) was strongly downregulated in both *eob2-3^{LofTAD}* floral organs compared to wild-type (Fig. 7b), suggesting that starch degradation was also impaired (Fig. 7c).

We next evaluated starch levels in wild-type vs *eob2-3^{LofTAD}* in both petals and nectaries using IKI staining. During wild-type flower development, we observed an accumulation of large amounts of starch at Stage S5 and decreased levels at stage 10, while starch levels remained high in *eob2-3^{LofTAD}* (Fig. 7d,e). In nectary at S10, starch was only detected within the wild-type stomata, whereas *eob2-3^{LofTAD}* nectary stained heavily for starch, comparable to S5 immature nectary (Fig. 7d). Full petal and petal limb epidermal peels, also revealed that *eob2-3^{LofTAD}* retained more starch granules compared to wild-type (Fig. 7e,f). In addition, *eob2-3^{LofTAD}* petal limb epidermal cells were smaller. The Lugol results were confirmed by starch content quantification (Fig. 7g). These results indicated that the carbohydrate breakdown was reduced in both nectary and limb of the *eob2-3^{LofTAD}* mutant (Fig. 7c). This is consistent with the juvenile character of the *eob2-3^{LofTAD}* mutant.

Discussion

Different promoter sequences and subtle differences in protein coding sequences drive the functional divergence of *EOB1* and *EOB2*

The *EOB1* and *EOB2* genes encode closely related members of subgroup 19 R2R3-MYB transcription factors. Nevertheless, *eob1* and *eob2* mutants display radically different phenotypes. Loss-of-function of *EOB1* causes a decrease in scent emission, whereas

EOB2 is extremely pleiotropic. Thus, there must be subtle differences in protein sequence and/or expression that are responsible for these highly distinct phenotypes. *EOB2* is expressed slightly earlier than *EOB1*, *EOB2* induces *EOB1* expression and a potential

EOB2-binding site is present in the *EOB1* promoter, potentially explaining their extremely similar expression patterns. Phylogenetic and microsynteny analysis reveal that species with a single SG19 member, the gene is closer to the petunia *EOB2* than to *EOB1*. It

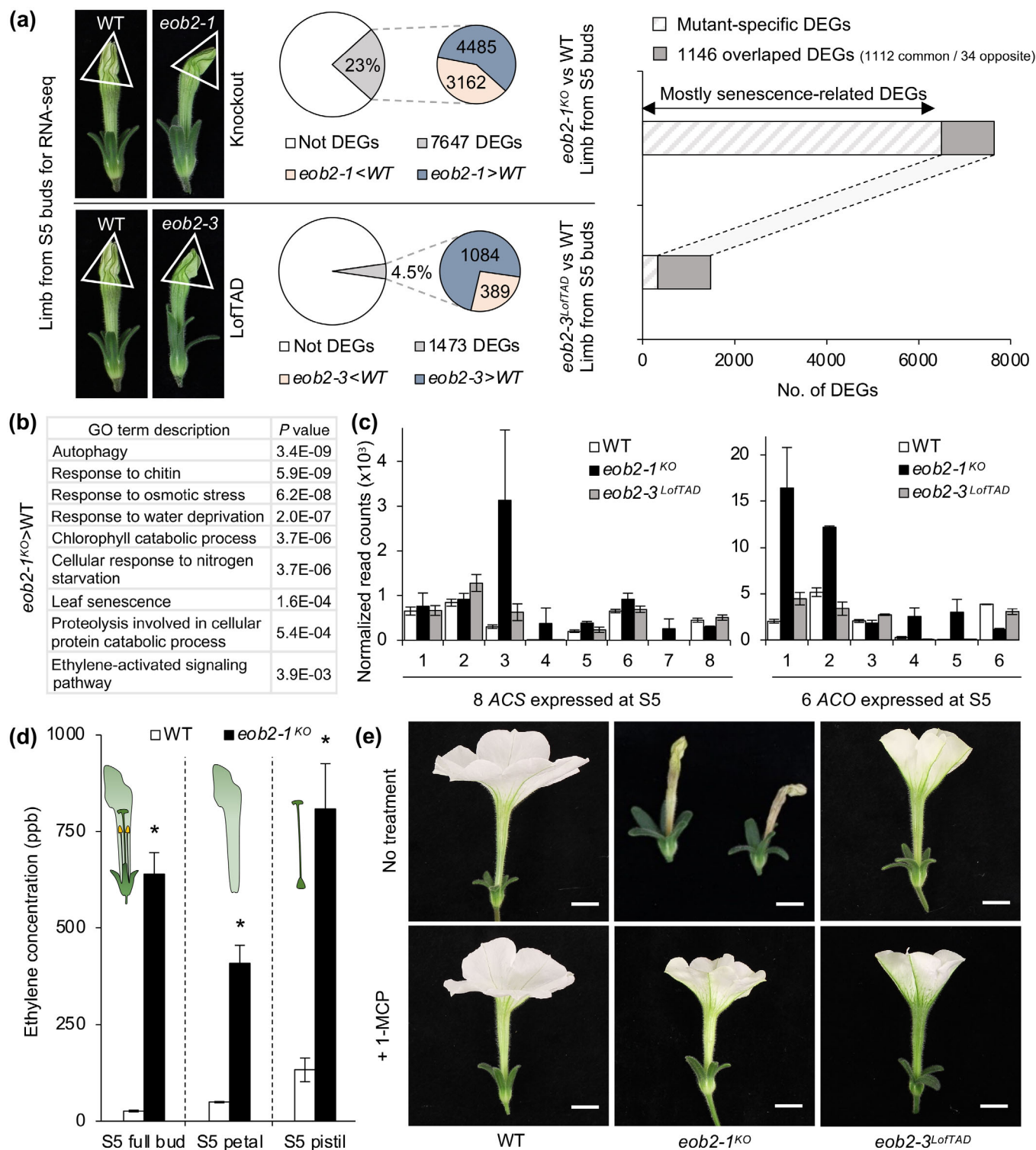


Fig. 5 Premature production of ethylene by flower buds is responsible for the knockout flower senescence phenotype. (a) RNA-seq experiment summary. Left: white triangles show the petal limb tissue part from S5 buds collected for the RNA-seq experiment (just before the first signs of senescence for *eob2-1^{KO}*). Middle: pie charts showing the proportion of DEGs in the *Petunia axillaris* transcriptome (total of 32 768 genes). Significant DEGs = $\log_2FC > 1$ or < -1 and *P*-adjusted value < 0.01 . Right: comparison of S5 limb total DEGs from *eob2-1^{KO}* vs WT and *eob2-3^{LoFTAD}* vs WT. (b) Gene ontology (GO) term enrichment analysis of specific up-regulated genes in *eob2-1^{KO}*. (c) RNA-seq results of genes belonging to ACS and ACO multi-gene families encoding for enzymes of the ethylene biosynthetic pathway. Only genes from the family expressed in either WT or *eob2-1* are shown (ACS 8/22 and ACO 6/13) (see Table S9 for gene ID). Error bars, SD. (d) Detection of ethylene released from WT and *eob2-1^{KO}* S5 full flower buds, S5 dissected petal or S5 dissected pistil, quantified using a laser-based photoacoustic ethylene sensor ($n = 30$ for WT and $n = 45$ for *eob2-1^{KO}*; error bars, SE; significant differences *, Students *t*-test: $P < 0.05$). Mutant samples were collected before the first signs of senescence, when the petal tips were still rigid. (e) Side view of flowers of WT, *eob2-1^{KO}* and *eob2-3^{LoFTAD}* with or without 1-MCP treatment. Partial rescue of the *eob2-1^{KO}* phenotype was observed. Bars, 1 cm.

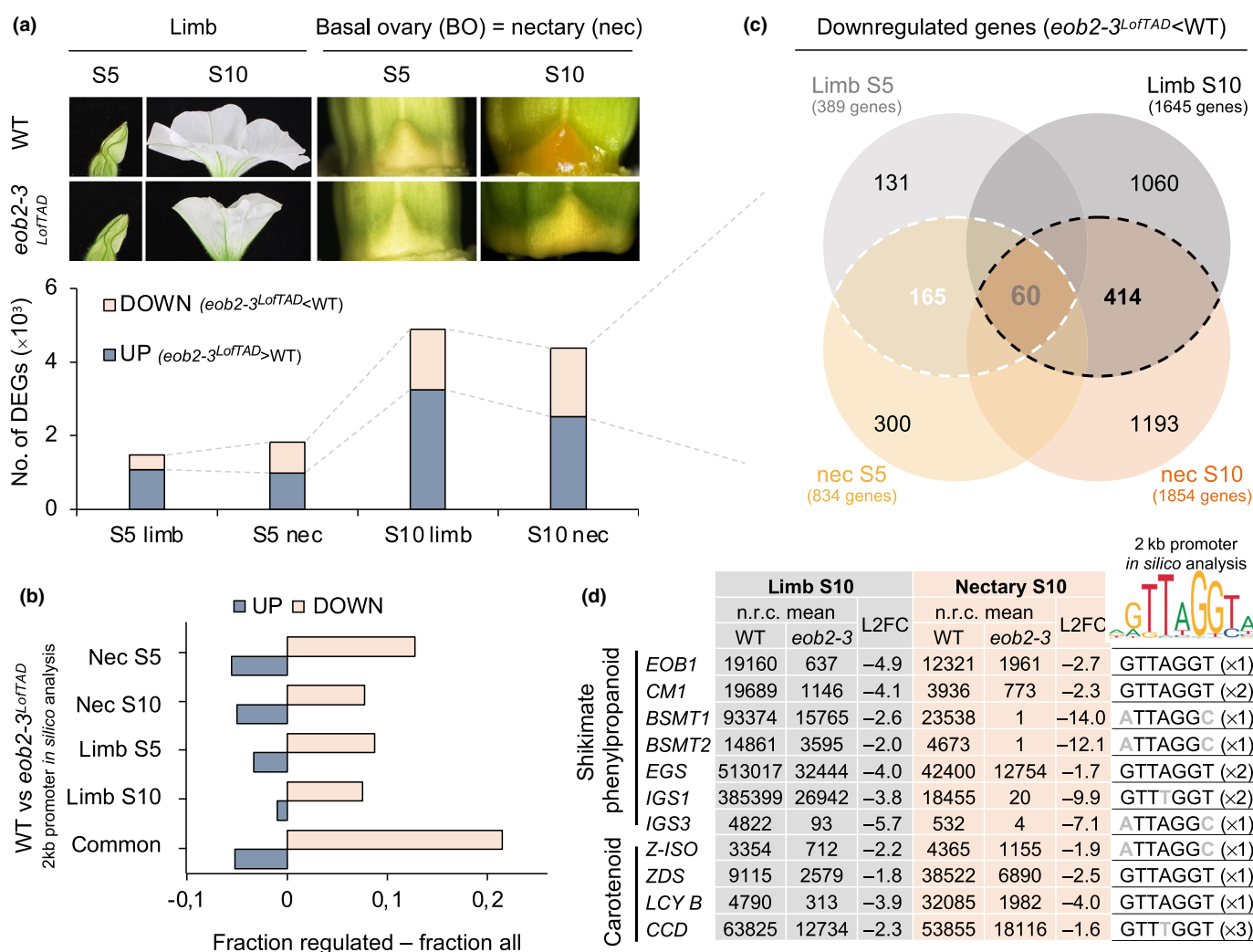


Fig. 6 *EOB2* activates the expression of common targets in two different floral organs. (a) RNA-seq experiment summary. Top: limb and basal ovary tissues collected just before dark at S5 and S10 for the RNA-seq experiment. Bottom: no. of DEGs between *eob2-3^{LoFTAD}* and WT. (b) The graph corresponds to the difference in fraction of genes (up vs all/down vs all) with a 2 kb promoter containing at least one putative R2R3-MYB SG19 binding site (matrix MA1408.1 (*FaEOB1*)). Similar results were obtained with MA1037.1 (*AtMYB24*) (Supporting Information Table S8). (c) Summary of overlaps between down-regulated genes (*eob2-3^{LoFTAD}* < WT) in limb and nectary at stages S5 and S10. (d) Table showing the expression data in limb and nectary at S10 of a selection of 11 genes over a total of 60 (from Fig. 6b). L2FC, Log₂ fold change; n.r.c., normalized read counts. The presence of a R2R3-MYB SG19 binding site in 2 kb promoter was predicted using FIMO. Motifs with grey nucleotides should also be recognized by SG19 proteins. BSMT, benzoic acid/salicylic acid carboxyl MethylTransferase; CM1, chorismate mutase 1; EGS, eugenol synthase; EOB1, emission of benzenoids 1; IGS, isoeugenol synthase. Carotenoid related: ζ-carotene isomerase (Z-ISO), ζ-carotene desaturase (ZDS), Lycopene Beta Cyclase (LCY B), Carotenoid cleavage dioxygenase (CCD). See Table S9 for gene ID.

might be that *EOB2* ancestor evolved as a driver of flower maturation, while *petunia EOB1* appeared later during evolution from *EOB2* duplication and gained a specific function in scent production (scent booster), notably due to its divergent promoter (Fig. S7)

and the associated delayed expression pattern compared to *EOB2*, with a peak at anthesis.

As *EOB1* expression was strongly reduced in an *eob2^{KO}* background, while *eob1^{KO}* mutants had normal *EOB2* expression,

EOB2 must be a major activator of *EOB1*. In parallel, a previous study revealed that PhERF6 interacts with EOB1 to regulate scent biosynthesis, but not with EOB2 (Liu *et al.*, 2017). Promoter differences and subtle differences in protein–protein interactions underlie the loss of scent phenotype in the *eob1*^{KO} mutant.

Nectary and limb are sink tissues that rely on common pathways for their maturation

At later developmental stages, the *LofTAD* mutant flowers retained starch, did not produce benzenoid/phenylpropanoid

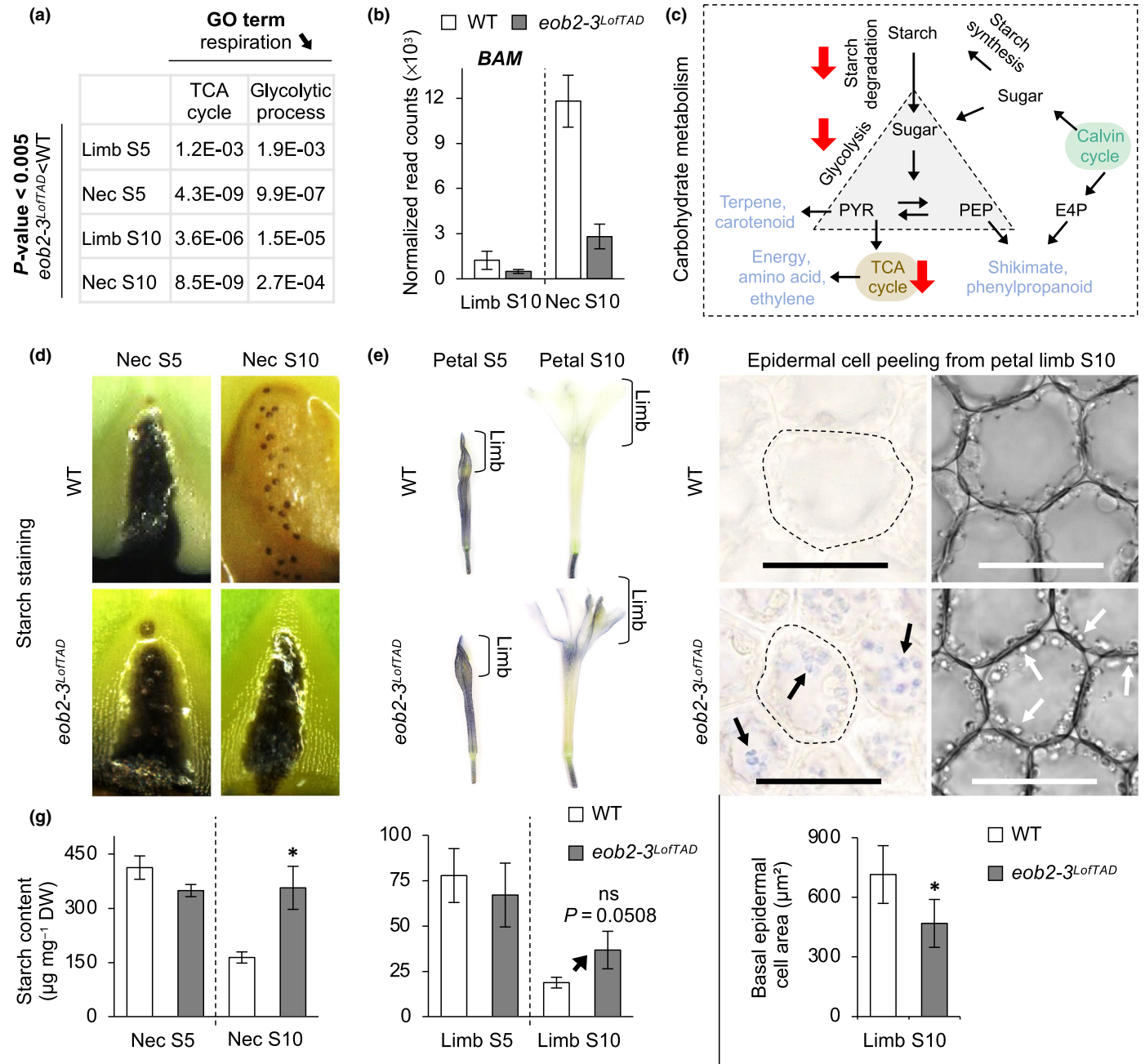


Fig. 7 Carbohydrate metabolism is disrupted in *eob2-3^{LofTAD}* nectary and limb. (a) GO terms from down-regulated genes co-enriched in *eob2-3^{LofTAD}* limb and nectary at S5 and S10 (P value < 0.005). (b) RNA-seq result of *BETA-AMYLASE* (*BAM*) in nectary and limb at S10. See Supporting Information Table S9 for gene ID. (c) Simplified representation of the carbohydrate metabolism pathway and the derived primary and secondary metabolites (blue). PYR, pyruvate; PEP, phosphoenolpyruvate; E4P, erythrose-4-phosphate; Rubisco, ribulose-1,5-bisphosphate carboxylase/oxygenase; TCA cycle, tricarboxylic acid cycle, also known as the Krebs cycle. (d) and (e) Visualization of starch in nectaries and cleared petal (S5 and S10) by staining with Lugol's solution. (f) Axial epidermal cell peeling from petal limb at S10. Left: Lugol's staining. Right: differential interference contrast (DIC) observation. Arrows indicate the starch granules inside the limb epidermal cells. Bars, 30 μm . Basal epidermal cell area (μm^2) of petal limb at S10 ($n = 90$ cells; error bars, SD; significant differences Student's t -test: *, $P < 0.05$). (g) Starch content in WT and *eob2-3^{LofTAD}* nectary and limb tissues at different stages. The black arrow indicates the tendency towards an accumulation of starch in *eob2-3^{LofTAD}* limb S10 compared to the WT ($n = 3$; error bars, SD; significant differences Student's t -test: *, $P < 0.05$; ns, non-significance).

volatiles, produced less terpenoids and presented a smaller, greener, not fully opened corolla (Figs 4, 7). In line with this, transcriptomic data revealed that genes encoding enzymes of both primary and secondary metabolisms were decreased in immature tissues compared to those of the WT. We consider following options: It could be that both primary and secondary metabolisms are dependent on EOB2 or that EOB2 directly regulates only one of these two processes and that the other process is reduced as a consequence. The presence of EOB2-binding sites in promoters of genes in the shikimate/phenylpropanoid and carotenoid pathways would support the second option. In that case, the decrease of energy-demanding secondary metabolites production could reduce carbohydrate flux through feedback inhibition.

Comparisons with the R2R3-MYB SG19 functions previously reported in the literature

In the **Introduction** section, we asked the question whether the conflicting data on the functions of SG19 R2R3-MYBs reported within and between different species were due to species specificity, to the methods used, to the focus of the study on a particular

organ or to the multifunctionality of the SG19 R2R3-MYBs. Here, we used well-defined mutants and revealed in a single system the complexity of the SG19 R2R3-MYB functions.

Comparable to *eob2* KO, premature flower senescence has been described for strong RNAi lines targeting *EOB2* homologs in *P. hybrida* and *N. attenuata* (Colquhoun *et al.*, 2011). By contrast and similar to *eob2* LofTAD, immature floral organ phenotypes were reported in other tobacco RNAi lines targeting *MYB305* (Liu *et al.*, 2009; Liu & Thornburg, 2012). We can speculate that those RNAi lines had an increased proportion of alternative splicing variants with an intact R2R3-MYB and no TAD (RNAi targeted the C-ter) or that the silencing was incomplete making it possible to block the senescence but not enough to induce transcription. The VIGS performed in *P. hybrida* targeting *EOB2* only revealed scent related phenotypes, so it could be that the silencing was incomplete or that *EOB1* instead of *EOB2* was targeted in this study.

The expression pattern of tobacco *MYB305* (Liu *et al.*, 2009) was similar to *Petunia* *EOB2*, while expression of Arabidopsis *AtMYB21* and *AtMYB24* was also detected in stamens and these proteins play a major role in Arabidopsis anther maturation (Qi *et al.*, 2015). Out of those different expression patterns and

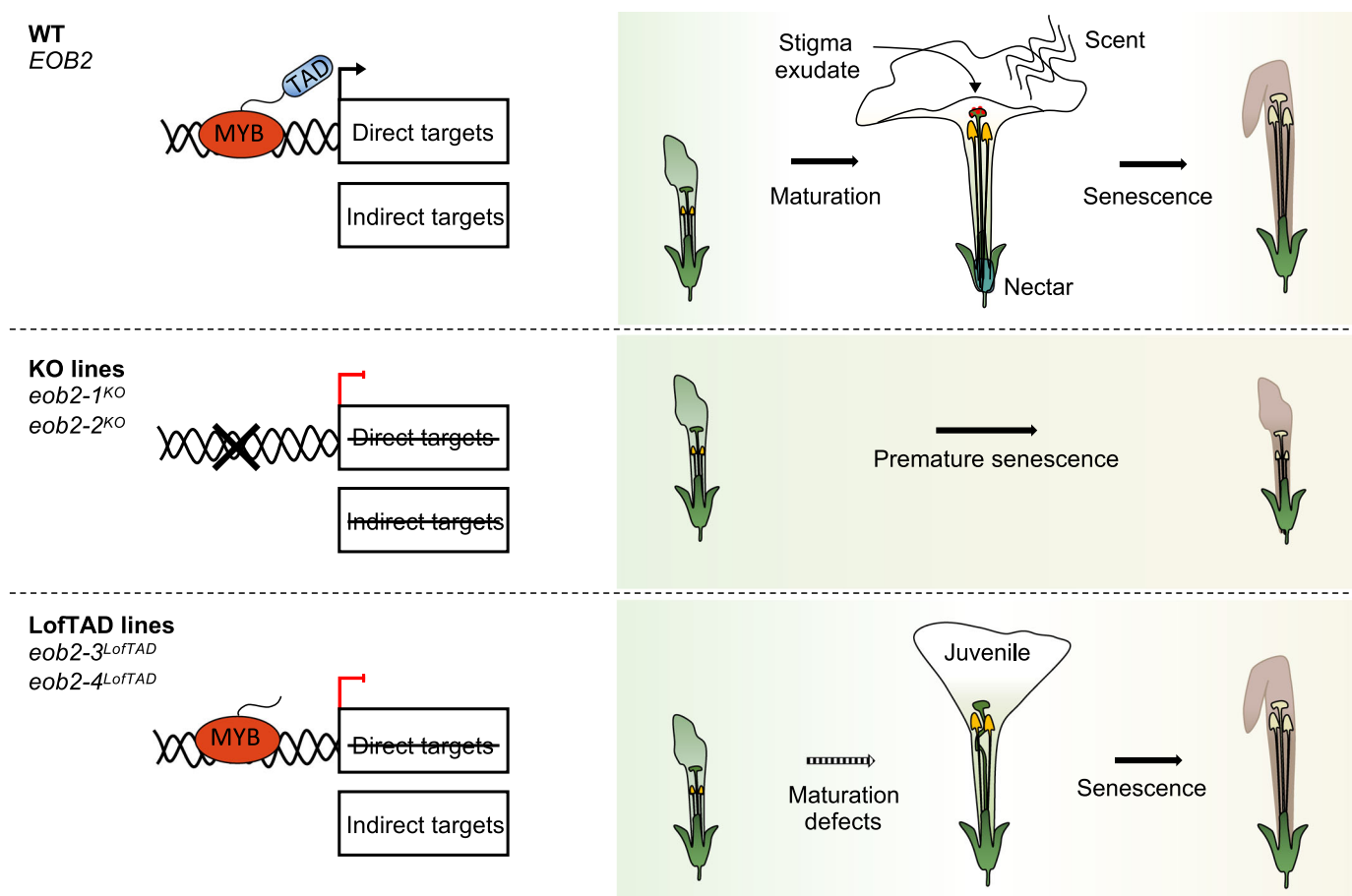


Fig. 8 One gene, two mutations, contrasting phenotypes. Model to illustrate EOB2 multi-functionality. The knockout (KO) lines and LofTAD lines do not present the same floral phenotype, while both lines are unable to activate target genes (represented by blunt-ended arrows). This is the proof that EOB2 is involved in other functions. Direct targets are most likely related to maturation-related genes like the secondary metabolism related genes, while indirect targets are probably senescence-related proteins/genes.

functions, we concluded that in *Arabidopsis* SG19 R2R3-MYB members were recruited for stamen maturation while other factors were selected in pollinator-dependent species such as *Petunia* or *Nicotiana*. Except for the stamens, *Arabidopsis* and *Petunia* SG19 genes have similar spatial expression patterns and share functions (nectary maturation, flower opening); however, other functions are specific for *Petunia* (senescence, FVBP) or for *Arabidopsis* (flavonols) (X. Zhang *et al.*, 2021). In addition to the differences in floral organ expression, it appears that during evolution, different partners and target genes were recruited by the SG19 R2R3-MYBs (Tables S1, S2).

One gene, two mutations, contrasting phenotypes

The *eob2*^{KO} mutations display premature flower senescence, whereas the semidominant *eob2*^{LofTAD} alleles retain the RMD^{SG19} functions specifically and *eob2*^{LofTAD} mutants and show multiple flower maturation defects resulting in juvenile flowers (Fig. 8). The conclusions are the following: (1) EOB2 is a multifunctional protein, (2) EOB2 transcriptional activity drives flower maturation, and (3) the R2R3-MYB domain is, in addition to its DNA-binding role in transcription, involved in the regulation of indirect senescence-related targets through an unknown mechanism. Cases of nonfunctional vs partially functional gene product showing different phenotypes are rare in the literature, an example is the tomato MADS-box gene *RIN* (for ripening inhibitor) where the *rin-knockout* (Ito *et al.*, 2017) and semi-dominant *rinG2* (Ito *et al.*, 2021) alleles were leading to different tomato fruit phenotypes. Proper conclusions about the function(s) of the protein require a careful analysis of the protein structure before targeting a TF gene by mutagenesis.

Complexity of SG19 MYB factors protein functions

The genetic processes that underlie the initiation and determination of the floral organs have been well-studied in *Arabidopsis*, snapdragon, and *Petunia* (Coen & Meyerowitz, 1991; Vandenbussche *et al.*, 2004; Morel *et al.*, 2018), and are quite well-conserved between species (Soltis *et al.*, 2007). Floral diversity mainly arises during subsequent maturation and serves to adapt flowers to specific guilds of pollinators (Schiestl & Johnson, 2013). This aspect may be negligible in a selfing species such as *Arabidopsis thaliana* but is essential in animal-pollinated species. The versatility of SG19 MYB factors and their many interacting regulatory factors appear to be well suited to adapt flowers for optimal pollination. SG19 MYB factors affect multiple aspects of flower maturation, with potential impact on the functions of the flower. These include floral morphology (Yarahmadov *et al.*, 2020), scent (Spitzer-Rimon *et al.*, 2010), nectar (Liu *et al.*, 2009, p. 305; Liu & Thornburg, 2012), and color (Wang *et al.*, 2022), but also plant defense against microorganisms mediated by the antimicrobial activity of terpenes (Boachon *et al.*, 2019) or compounds present in the stigma exudate/nectar (Kurilla *et al.*, 2019).

While part of the confusion about the roles of SG19 MYB factors in flower development may be due to the use of different

techniques, it is also clear that data on EOB2 and its homologs cannot be extrapolated from one species to the next, possibly reflecting the diversity of plant–pollinator interactions.

Acknowledgements

This work was supported by grants from the Swiss National Science Foundation (31003A_182340) and the European Union (ERC-ADG 741354). We would like to thank the Next Generation Sequencing Platform of the University of Bern for performing the high-throughput sequencing experiments and the Interfaculty Bioinformatics Unit of the University of Bern for providing computational infrastructure and support with bioinformatic analyses. We thank Christopher Ball, Jasmin Sekulovski, and Sarah Dolder for taking care of our *Petunia* plants. We are grateful to Patrick Ryan and Ying Li for providing their GO annotations, Diane Bonnet for advice on microscopy, Aya Assamene for technical support, and Chaobin Li for bioinformatics supports as well as helpful discussion and proof-reading. Open access funding provided by Universitat Bern.










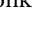
Competing interests

None declared.

Author contributions

MC and CK conceived and designed the experiments. MC generated the CRISPR-Cas9 lines, performed the phenotyping/pictures, the 1-MCP treatments, the starch staining using Lugol, the RT-qPCR with the technical support of LJ. GC performed the protein structures prediction with ALPHAFOLD. R Halitschke performed the ethylene measurements. BB and DPB performed the terpene measurements. R Heutink and JCV performed the starch and carotenoid measurements. MC, MB and GG performed the RNA-seq analysis. MC and CK wrote the article.

ORCID

Marta Binaghi  <https://orcid.org/0000-0001-6951-792X>
Benoît Boachon  <https://orcid.org/0000-0002-2362-2238>
Dikki Pedenla Bomzan  <https://orcid.org/0000-0003-0595-0569>
Gina Cannarozzi  <https://orcid.org/0000-0002-0704-663X>
Mathilde Chopy  <https://orcid.org/0000-0003-4403-5769>
Geert van Geest  <https://orcid.org/0000-0002-1561-078X>
Rayko Halitschke  <https://orcid.org/0000-0002-1109-8782>
Roel Heutink  <https://orcid.org/0000-0002-6084-2395>
Cris Kuhlemeier  <https://orcid.org/0000-0003-2440-5937>
Julian C. Verdonk  <https://orcid.org/0000-0002-1237-7951>

Data availability

Raw reads are available on NCBI Sequence Read Archive (SRA), under the BioProject accession no. PRJNA797226 (reviewer link:

<https://dataview.ncbi.nlm.nih.gov/object/PRJNA797226?reviewer=pa7i8vmprfq6vvu67ui6tqvju>). Plasmids and seeds produced in this study are available from CK on request.

References

- Amrad A, Moser M, Mandel T, de Vries M, Schuurink RC, Freitas L, Kuhlmeier C. 2016. Gain and loss of floral scent production through changes in structural genes during pollinator-mediated speciation. *Current Biology* 26: 3303–3312.
- Andrews S. 2010. *Babraham bioinformatics – FASTQC a quality control tool for high throughput sequence data*. <https://www.bibsonomy.org/bibtex/f230a919c34360709aa298734d63dc3a>
- Battat M, Eitan A, Rogachev I, Hanhineva K, Fernie A, Tohge T, Beekwilder J, Aharoni A. 2019. A MYB triad controls primary and phenylpropanoid metabolites for pollen coat patterning. *Plant Physiology* 180: 87–108.
- Bian S, Sui X, Wang J, Tian T, Wang C, Zhao X, Liu X, Fang N, Zhang Y, Liu Y *et al.* 2021. NtMYB305a binds to the jasmonate-responsive GAG region of NtPMT1a promoter to regulate nicotine biosynthesis. *Plant Physiology* 188: 151–166.
- Boachon B, Lynch J, Ray S, Yuan J, Caldo K, Junker R, Kessler S, Morgan J, Dudareva N. 2019. Natural fumigation as a mechanism for volatile transport between flower organs. *Nature Chemical Biology* 15: 583–588.
- Brandenburg A, Kuhlmeier C, Bshary R. 2012. Hawkmoth pollinators decrease seed set of a low-nectar *Petunia axillaris* line through reduced probing time. *Current Biology* 22: 1635–1639.
- Cheng H, Song S, Xiao L, Soo HM, Cheng Z, Xie D, Peng J. 2009. Gibberellin acts through jasmonate to control the expression of MYB21, MYB24, and MYB57 to promote stamen filament growth in Arabidopsis. *PLoS Genetics* 5: e1000440.
- Chopy M, Morel P, Rodrigues Bento S, Vandenbussche M. 2020. Genome editing by CRISPR-Cas9 technology in *Petunia hybrida*. *Acta Horticulturae* 1283: 209–218.
- Coen ES, Meyerowitz EM. 1991. The war of the whorls: genetic interactions controlling flower development. *Nature* 353: 31–37.
- Colquhoun TA, Schwieterman ML, Wedde AE, Schimmel BCJ, Marciniak DM, Verdonk JC, Kim JY, Oh Y, Galis I, Baldwin IT *et al.* 2011. EOBII controls flower opening by functioning as a general transcriptomic switch. *Plant Physiology* 156: 974–984.
- Edgar RC. 2004. MUSCLE: multiple sequence alignment with high accuracy and high throughput. *Nucleic Acids Research* 32: 1792–1797.
- Edwards K, Johnstone C, Thompson C. 1991. A simple and rapid method for the preparation of plant genomic DNA for PCR analysis. *Nucleic Acids Research* 19: 1349.
- Grant CE, Bailey TL, Noble WS. 2011. FIMO: scanning for occurrences of a given motif. *Bioinformatics* 27: 1017–1018.
- Guindon S, Dufayard J-F, Lefort V, Anisimova M, Hordijk W, Gascuel O. 2010. New algorithms and methods to estimate maximum-likelihood phylogenies: assessing the performance of PHYML 3.0. *Systematic Biology* 59: 307–321.
- Hoballah ME, Stuurman J, Turlings TCJ, Guerlin PM, Connétable S, Kuhlmeier C. 2005. The composition and timing of flower odour emission by wild *Petunia axillaris* coincide with the antennal perception and nocturnal activity of the pollinator *Manduca sexta*. *Planta* 222: 141–150.
- Huang H, Gao H, Liu B, Qi T, Tong J, Xiao L, Xie D, Song S. 2017. Arabidopsis MYB24 regulates jasmonate-mediated stamen development. *Frontiers in Plant Science* 8: 1525.
- Huang H, Gong Y, Liu B, Wu D, Zhang M, Xie D, Song S. 2020. The DELLA proteins interact with MYB21 and MYB24 to regulate filament elongation in Arabidopsis. *BMC Plant Biology* 20: 64.
- Ito Y, Nakamura N, Kotake-Nara E. 2021. Semi-dominant effects of a novel ripening inhibitor (rin) locus allele on tomato fruit ripening. *PLoS ONE* 16: e0249575.
- Ito Y, Nishizawa-Yokoi A, Endo M, Mikami M, Shima Y, Nakamura N, Kotake-Nara E, Kawasaki S, Toki S. 2017. Re-evaluation of the rin mutation and the role of RIN in the induction of tomato ripening. *Nature Plants* 3: 866–874.
- Jumper J, Evans R, Pritzel A, Green T, Figurnov M, Ronneberger O, Tunyasuvunakool K, Bates R, Židek A, Potapenko A *et al.* 2021. Highly accurate protein structure prediction with AlphaFold. *Nature* 596: 583–589.
- Ke Y, Abbas F, Zhou Y, Yu R, Fan Y. 2021. Auxin-responsive R2R3-MYB transcription factors HcMYB1 and HcMYB2 activate volatile biosynthesis in *Hedychium coronarium* flowers. *Frontiers in Plant Science* 12: 710826.
- Kim D, Langmead B, Salzberg SL. 2015. HISAT: a fast spliced aligner with low memory requirements. *Nature Methods* 12: 357–360.
- Kosugi S, Hasebe M, Tomita M, Yanagawa H. 2009. Systematic identification of cell cycle-dependent yeast nucleocytoplasmic shuttling proteins by prediction of composite motifs. *Proceedings of the National Academy of Sciences, USA* 106: 10171–10176.
- Kurilla A, Toth T, Dorgai L, Darula Z, Lakatos T, Silhavy D, Kerenyi Z, Dallmann G. 2019. Nectar- and stigma exudate-specific expression of an acidic chitinase could partially protect certain apple cultivars against fire blight disease. *Planta* 251: 20.
- Liao Y, Smyth GK, Shi W. 2014. FEATURECOUNTS: an efficient general purpose program for assigning sequence reads to genomic features. *Bioinformatics* 30: 923–930.
- Liu F, Xiao Z, Yang L, Chen Q, Shao L, Liu J, Yu Y. 2017. PhERF6, interacting with EOB1, negatively regulates fragrance biosynthesis in *Petunia* flowers. *New Phytologist* 215: 1490–1502.
- Liu G, Ren G, Guirgis A, Thornburg RW. 2009. The MYB305 transcription factor regulates expression of nectarin genes in the ornamental tobacco floral nectary. *Plant Cell* 21: 2672–2687.
- Liu G, Thornburg RW. 2012. Knockdown of MYB305 disrupts nectary starch metabolism and floral nectar production. *The Plant Journal* 70: 377–388.
- Love MI, Huber W, Anders S. 2014. Moderated estimation of fold change and dispersion for RNA-seq data with DESeq2. *Genome Biology* 15: 550.
- Lyons E, Pedersen B, Kane J, Alam M, Ming R, Tang H, Wang X, Bowers J, Paterson A, Lisch D *et al.* 2008. Finding and comparing syntenic regions among Arabidopsis and the outgroups papaya, poplar, and grape: CoGe with Rosids. *Plant Physiology* 148: 1772–1781.
- Ma D, Constabel CP. 2019. MYB repressors as regulators of phenylpropanoid metabolism in plants. *Trends in Plant Science* 24: 275–289.
- Mallona I, Lischewski S, Weiss J, Hause B, Egea-Cortines M. 2010. Validation of reference genes for quantitative real-time PCR during leaf and flower development in *Petunia hybrida*. *BMC Plant Biology* 10: 4.
- Mandaokar A, Thines B, Shin B, Lange BM, Choi G, Koo YJ, Yoo YJ, Choi YD, Choi G, Browse J. 2006. Transcriptional regulators of stamen development in Arabidopsis identified by transcriptional profiling. *The Plant Journal* 46: 984–1008.
- Martin M. 2011. Cutadapt removes adapter sequences from high-throughput sequencing reads. *EMBnet.journal* 17: 10–12.
- Medina-Puche L, Molina-Hidalgo FJ, Boersma M, Schuurink RC, López-Vidriero I, Solano R, Franco-Zorrilla J-M, Caballero JL, Blanco-Portales R, Muñoz-Blanco J. 2015. An R2R3-MYB transcription factor regulates eugenol production in ripe strawberry fruit receptacles. *Plant Physiology* 168: 598–614.
- Moerkercke AV, Haring MA, Schuurink RC. 2011. The transcription factor EMISSION OF BENZENOIDES II activates the MYB ODORANT1 promoter at a MYB binding site specific for fragrant petunias. *The Plant Journal* 67: 917–928.
- Morel P, Heijmans K, Ament K, Chopy M, Trehin C, Chambrier P, Bento SR, Bimbo A, Vandenbussche M. 2018. The Floral C-lineage genes trigger nectary development in *Petunia* and Arabidopsis. *Plant Cell* 30: 2020–2037.
- Moyano E, Martínez-García JF, Martín C. 1996. Apparent redundancy in myb gene function provides gearing for the control of flavonoid biosynthesis in antirrhinum flowers. *Plant Cell* 8: 1519–1532.
- Nakagawa T, Suzuki T, Murata S, Nakamura S, Hino T, Maeo K, Tabata R, Kawai T, Tanaka K, Niwa Y *et al.* 2007. Improved gateway binary vectors: high-performance vectors for creation of fusion constructs in transgenic analysis of plants. *Bioscience, Biotechnology, and Biochemistry* 71: 2095–2100.
- Niwa T, Suzuki T, Takebayashi Y, Ishiguro R, Higashiyama T, Sakakibara H, Ishiguro S. 2018. Jasmonic acid facilitates flower opening and floral organ development through the upregulated expression of SIMYB21

- transcription factor in tomato. *Bioscience, Biotechnology, and Biochemistry* 82: 292–303.
- Okonechnikov K, Golosova O, Fursov M, the UGENE team. 2012. UNIPRO UGENE: a unified bioinformatics toolkit. *Bioinformatics* 28: 1166–1167.
- Patrick RM, Huang X-Q, Dudareva N, Li Y. 2021. Dynamic histone acetylation in floral volatile synthesis and emission in petunia flowers. *Journal of Experimental Botany* 72: 3704–3722.
- Qi T, Huang H, Song S, Xie D. 2015. Regulation of jasmonate-mediated stamen development and seed production by a bHLH-MYB complex in *Arabidopsis*. *Plant Cell* 27: 1620–1633.
- Reeves PH, Ellis CM, Ploense SE, Wu M-F, Yadav V, Tholl D, Chételat A, Haupt I, Kennerley BJ, Hodgins C *et al.* 2012. A regulatory network for coordinated flower maturation. *PLoS Genetics* 8: e1002506.
- Sablowski RW, Moyano E, Culianez-Macia FA, Schuch W, Martin C, Bevan M. 1994. A flower-specific Myb protein activates transcription of phenylpropanoid biosynthetic genes. *EMBO Journal* 13: 128–137.
- Schiestl FP, Johnson SD. 2013. Pollinator-mediated evolution of floral signals. *Trends in Ecology & Evolution* 28: 307–315.
- Schmitt AJ, Roy R, Klinkenberg PM, Jia M, Carter CJ. 2018. The octadecanoid pathway, but not COI1, is required for nectar secretion in *Arabidopsis thaliana*. *Frontiers in Plant Science* 9: 1060.
- Schubert R, Dobritsch S, Gruber C, Hause G, Athmer B, Schreiber T, Marillonnet S, Okabe Y, Ezura H, Acosta IF *et al.* 2019. Tomato MYB21 acts in ovules to mediate jasmonate-regulated fertility. *Plant Cell* 31: 1043–1062.
- Shan X, Li Y, Yang S, Yang Z, Qiu M, Gao R, Han T, Meng X, Xu Z, Wang L *et al.* 2020. The spatio-temporal biosynthesis of floral flavonols is controlled by differential phylogenetic MYB regulators in *Freesia hybrida*. *New Phytologist* 228: 1864–1879.
- Soltis DE, Chanderbali AS, Kim S, Buzgo M, Soltis PS. 2007. The ABC model and its applicability to basal angiosperms. *Annals of Botany* 100: 155–163.
- Song S, Qi T, Huang H, Ren Q, Wu D, Chang C, Peng W, Liu Y, Peng J, Xie D. 2011. The jasmonate-ZIM domain proteins interact with the R2R3-MYB transcription factors MYB21 and MYB24 to affect jasmonate-regulated stamen development in *Arabidopsis*. *Plant Cell* 23: 1000–1013.
- Spitzer-Rimon B, Farhi M, Albo B, Cna'ani A, Zvi MMB, Masci T, Edelbaum O, Yu Y, Shklarman E, Ovadis M *et al.* 2012. The R2R3-MYB-like regulatory factor EOB1, acting downstream of EOBII, regulates scent production by activating ODO1 and structural scent-related genes in *Petunia*. *Plant Cell* 24: 5089–5105.
- Spitzer-Rimon B, Marheva E, Barkai O, Marton I, Edelbaum O, Masci T, Prathapani N-K, Shklarman E, Ovadis M, Vainstein A. 2010. EOBII, a gene encoding a flower-specific regulator of phenylpropanoid volatiles' biosynthesis in *Petunia*. *Plant Cell* 22: 1961–1976.
- Streb S, Zeeman SC. 2012. Starch metabolism in *Arabidopsis*. *The Arabidopsis Book/American Society of Plant Biologists* 10: e0160.
- Van Geest G, Choi YH, Arens P, Post A, Liu Y, Van Meeteren U. 2016. Genotypic differences in metabolomic changes during storage induced-degreening of chrysanthemum disk florets. *Postharvest Biology and Technology* 115: 48–59.
- Van Moerkercke A, Galván-Ampudia CS, Verdonk JC, Haring MA, Schuurink RC. 2012. Regulators of floral fragrance production and their target genes in *petunia* are not exclusively active in the epidermal cells of petals. *Journal of Experimental Botany* 63: 3157–3171.
- Vandenbussche M, Zethof J, Royaert S, Weterings K, Gerats T. 2004. The duplicated B-class heterodimer model: whorl-specific effects and complex genetic interactions in *Petunia hybrida* flower development. *Plant Cell* 16: 741–754.
- Wang Y, Zhou L-J, Wang Y, Geng Z, Ding B, Jiang J, Chen S, Chen F. 2022. An R2R3-MYB transcription factor CmMYB21 represses anthocyanin biosynthesis in color fading petals of chrysanthemum. *Scientia Horticulturae* 293: 110674.
- Weirauch MT, Yang A, Albu M, Cote AG, Montenegro-Montero A, Drewe P, Najafabadi HS, Lambert SA, Mann I, Cook K *et al.* 2014. Determination and inference of eukaryotic transcription factor sequence specificity. *Cell* 158: 1431–1443.
- Wu T, Hu E, Xu S, Chen M, Guo P, Dai Z, Feng T, Zhou L, Tang W, Zhan L *et al.* 2021. CLUSTERPROFILER 4.0: a universal enrichment tool for interpreting omics data. *The Innovations* 2: 100141.
- Wu Z, Li T, Liu X, Yuan G, Hou H, Teng N. 2021. A novel R2R3-MYB transcription factor LfMYB305 from *Lilium longiflorum* plays a positive role in thermotolerance via activating heat-protective genes. *Environmental and Experimental Botany* 184: 104399.
- Yang Z, Li Y, Gao F, Jin W, Li S, Kimani S, Yang S, Bao T, Gao X, Wang L. 2020. MYB21 interacts with MYC2 to control the expression of terpene synthase genes in flowers of *Freesia hybrida* and *Arabidopsis thaliana*. *Journal of Experimental Botany* 71: 4140–4158.
- Yarahmadv T, Robinson S, Hanemian M, Pulver V, Kuhlmeier C. 2020. Identification of transcription factors controlling floral morphology in wild *Petunia* species with contrasting pollination syndromes. *The Plant Journal* 104: 289–301.
- Zhang C, Dai Z, Ferrier T, Matus JT. 2021. The grape MYB24 mediates the coordination of light-induced terpene and flavonol accumulation in response to berry anthocyanin sunscreen depletion. *Preprint bioRxiv*. doi: 10.1101/2021.12.16.472692.
- Zhang X, He Y, Li L, Liu H, Hong G. 2021. Involvement of the R2R3-MYB transcription factor MYB21 and its homologs in regulating flavonol accumulation in *Arabidopsis* stamen. *Journal of Experimental Botany* 72: 4319–4332.

Supporting Information

Additional Supporting Information may be found online in the Supporting Information section at the end of the article.

Fig. S1 Multiple sequence alignment of SG19 R2R3-MYB proteins.

Fig. S2 Microsynteny analysis comparing genomic regions surrounding *EOB1* or *EOB2* in *Petunia axillaris* and *Solanum lycopersicum*.

Fig. S3 Description of the different *Petunia axillaris* P floral developmental stages used in this study.

Fig. S4 Construction of *eob1* and *eob2* mutant alleles by CRISPR-Cas9.

Fig. S5 Observation of the internal floral organs of *eob2-1^{KO}* and *eob2-2^{KO}* flower buds.

Fig. S6 *eob2-3LofTAD* and *eob2-4LofTAD* are semidominant alleles.

Fig. S7 *EOB1* and *EOB2* promoter sequences are highly divergent.

Fig. S8 Additional phenotyping of *eob2-3^{LofTAD}*.

Fig. S9 Branches of WT, *eob2-1^{KO}* and *eob2-2^{KO}* before and after 1-MCP treatment.

Fig. S10 *eob2-1^{KO}* and *eob2-2^{KO}* flowers after 1-MCP treatment looked similar to *eob2-3^{LofTAD}* and *eob2-4^{LofTAD}*.

Fig. S11 Percentage of genes with a 2 kb promoter containing at least one putative R2R3-MYB SG19 binding site.

Fig. S12 Model showing the direct activation of secondary metabolite related genes by EOB2.

Methods S1 Quantification of sesquiterpene accumulation in *Petunia* pistils and emission from tube by GC–MS.

Methods S2 Carotenoid extraction and quantification with an HPLC system.

Methods S3 Starch extraction and quantification with an HPLC system.

Table S1 Summary of protein–protein interactions involving members of the R2R3-MYB SG19 reported in the literature.

Table S2 Summary of the direct target genes of members of the R2R3-MYB SG19 reported in the literature.

Table S3 gRNA sequences used to target EOB1 and EOB2.

Table S4 Sequence description of primers used for this work.

Table S5 Description of the samples collected for the RNA sequencing experiment.

Table S6 Description of the samples collected for the starch and carotenoid measurements.

Table S7 From the T0 transgenic lines obtained by CRISPR-Cas9 to the final homozygous mutant lines used in this study.

Table S8 Fraction of genes with a 2 kb promoter containing at least one putative R2R3-MYB SG19 binding site.

Table S9 Gene ID of genes used in this study.

Please note: Wiley is not responsible for the content or functionality of any Supporting Information supplied by the authors. Any queries (other than missing material) should be directed to the *New Phytologist* Central Office.